5-2014

Analysis and Mitigation of Impacts of Plug-In Electric Vehicles on Distribution System During Faults

Himanshu Bihani
Clemson University, bihani.himanshu@gmail.com

ANALYSIS AND MITIGATION OF IMPACTS OF PLUG-IN ELECTRIC VEHICLES ON DISTRIBUTION SYSTEM DURING FAULTS

A Thesis
Presented to
the Graduate School of
Clemson University

In Partial Fulfillment
of the Requirements for the Degree
Master of Science
Electrical Engineering

---

by
Himanshu Ashok Bihani
May 2014

Accepted by:
Dr. Elham Makram, Committee Chair
Dr. John N. Gowdy
Dr. Richard E. Groff

ABSTRACT

With rising concerns for environment, energy security and gasoline prices, penetration of plug-in electric vehicles (PEV) is bound to increase in the distribution system. The load characteristics of the distribution system with PEVs will be considerably different and hence its effects on the system needs to evaluated. Determination of the characteristics of the impacts will help utilities to prepare methodologies in advance to accommodate this new kind of load. Batteries of most of these vehicles will be charged using a single phase power electronic chargers. To study impact of these chargers on distribution system during fault and fault recovery is the focus of this thesis. The IEEE 13 node test feeder and a single phase Level-2 battery charging system with current controlled and voltage controlled Voltage Source Converter (VSC) is modeled in PSCAD™/EMTDC™. A car park, with sixteen PEVs, each rated for 6.6 kW, is connected on each of the three phases, at one of the buses in the system. Temporary single line to ground fault (SLG) with auto-reclosure operation is simulated at the bus where the vehicles are connected. The response of the systems in terms of active and reactive power flows, voltage and current magnitudes is evaluated. Based on the observations, the charger is equipped with fault control logic and fault studies are repeated to gage its effectiveness.

ACKNOWLEDGMENTS

I would like to take this opportunity to express my gratitude to my advisor, Dr. Elham Makram for her support, guidance and the wonderful working atmosphere she provided which made the journey to completion of my research and study at Clemson University a memorable experience.

I wish to thank Dr. Richard Groff and Dr. John N. Gowdy for accepting to be my committee members.

I also wish to thank Dr. Keith Corzine for his help and time he devoted from his busy schedule for guiding me throughout the course of this research.

Last but not the least I would like to thank all my colleagues at Clemson University for all the wonderful discussions we had together. My special thanks to Mr. Andrew Clarke for sharing his data base accessing code. It helped me to a great extent to manage the deluge of data generated during the course of this research.

TABLE OF CONTENTS

Table of Contents (Continued)

LIST OF TABLES

Table Page

LIST OF FIGURES

Figure Page

LIST OF FIGURES (CONTINUED)

CHAPTER ONE

BATTERY CHARGING SYSTEM AND CURRENT CONTROLLED VOLTAGE SOURCE CONVERTER TYPE OF BATTERY CHARGER

1.1 Introduction to Battery Charging System:

At present, the transportation sector is heavily dependent on petroleum based fuels. In order to address the concerns associated with these, efforts are being made to develop alternative fuel sources for the vehicles. These concerns deal with economics, energy security, and the environment. Plug-In Electric Vehicles (PEVs) that incorporate electric propulsion unit is the technology meant to reduce the dependence on petroleum based fuels. As battery technology continues to improve, market projections for PEVs are promising [1]. [2]

Based on the components involved in its drivetrain, PEVs can be classified as Battery Electric Vehicle (BEV), Plug-In Hybrid Electric Vehicle (PHEV) and Extended Range Electric Vehicle (EREV) [3]. BEVs depends only on a battery pack to meet all of its power requirements. Of all the types of PEVs, BEVs have the highest all electric range of about 60 to 100 miles and the largest battery capacity of about 25-35 kWh. The present day examples of BEVs are Nissan Leaf and Tesla Roadster. Both PHEVs and EREVs contain a battery pack and a gasoline engine to meets its power requirements. The main difference between the two is that a PHEV relies mainly on the gasoline engine whereas in case of an EREV, most of the energy from the battery pack is exhausted first before switching to the gasoline fuel. A typical all electric driving range of an EREV is about 40-

60 miles. Present day example of an EREV is Chevrolet Volt while that of a PHEV is Toyota Prius with plug-in capability [3].

The charging methods in North America are shown in Table 1.1. Based on the available infrastructure the batteries can be charged using AC Level 1 and AC Level 2 [4].

Table 1.1- Charging Methods In North America [4]

Charging Method	Nominal Supply Voltage	Max. Current	Continues Input Power
AC Level 1	120 V,1ph	12 A	1.44 kW
AC Level 2	208 - 240 V, 1ph	32 A	6.66 to 7.68 kW
AC Level 3	208 – 600 V, 3ph	400 A	>7.68 kW
DC Charging	600 V Max.	400 A	<240 kW

PEV batteries contain interconnected battery modules which encompass individual battery cells. These battery cells are connected in series and parallel combination based on the voltage and current rating requirements. Most commonly used batteries for PEV applications are lead acid, nickel metal hydride (NiMH) and lithium-ion (Li-Ion) batteries [5]. Li-Ion batteries, due to their higher cell voltage and higher energy density per unit volume, are the most viable option of energy storage for the present generation of the PEVs [6]. Higher cell voltage necessitate fewer cells to be connected in series for a given voltage requirement and higher energy density facilitate smaller battery packs. The most common charging profile used for Li-Ion batteries is Constant Current (CC) and Constant Voltage (CV) charging [5]. During constant current charging, the current is regulated at a constant value until the cell voltage reaches a certain value. Generally, CC charging continues until State of Charge (SOC) of the battery reaches to about 75%. The charging is then switched to CV charging and the battery is charged with trickle current applied by

constant voltage output of the charger. The duration of CC charging varies based on cathode composition of the Li-Ion battery. For Li-Ion batteries with lithium-cobalt-oxide cathode composition (LCO), which is widely used in consumer applications, CC charging consumes 25% of the total charging time to charge the battery up to 75% of its SOC. While in case of Li-Ion batteries with lithium-iron-phosphate cathode composition (LFP), which is widely used in automotive applications, CC charging consumes 75% of the total charging time [5]. Typical CC-CV characteristic of LFP cell is as shown in Fig. 1.1.

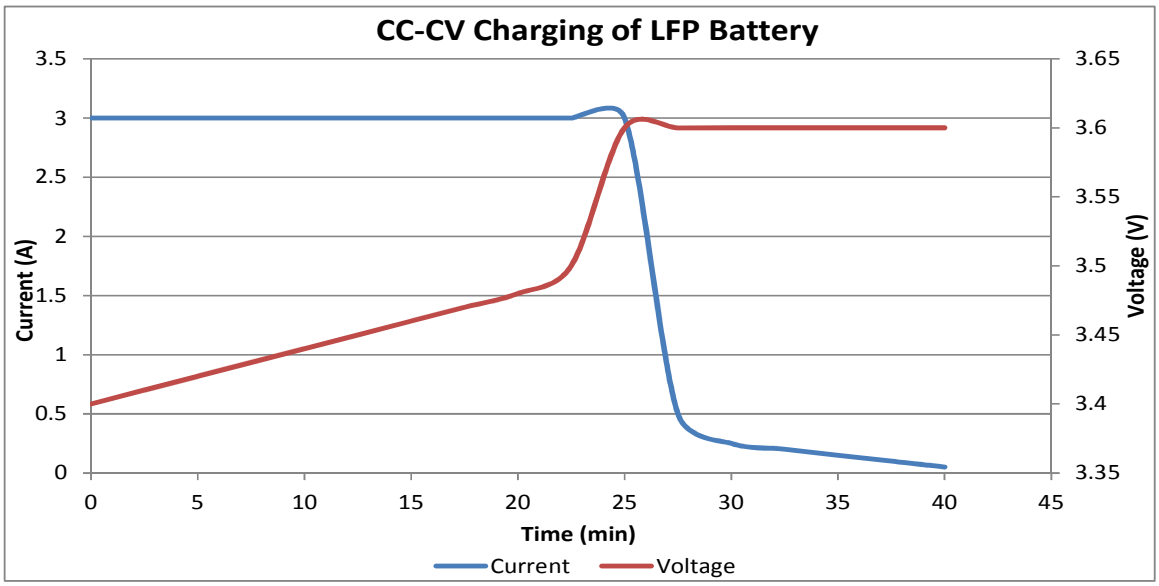

Fig. 1.1- CC-CV Charging Characteristic of LFP Type Li-Ion Battery Cell [5]

The power electronics and the associated control of the battery charging system is the technology that will make PEV integration feasible. As opposed to the common belief, the problems associated with the power electronics are much more challenging than the current battery technology [7]. Considerable research has already been done in the field of unidirectional as well as bidirectional battery chargers which comply with grid interfacing requirements [4, 8-12]. These chargers mainly differ in their topology and/or their control

methodology. The generalized topology for a single phase bidirectional charger can be represented as shown in Fig. 1.2.

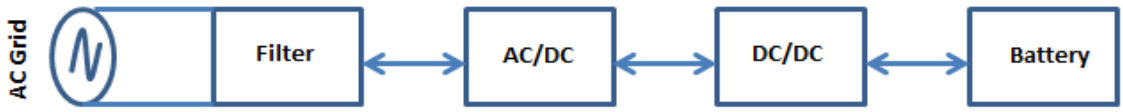

Fig. 1.2- General Block Diagram Of A Single Phase PEV Charger [13]

1.2 Charging of Lithium- Ion Batteries and Modeling of Battery Chargers:

1.2.1 Charging of Lithium- Ion Batteries:

Li-Ion battery model provided by PSCAD™/EMTDC™ customer support was used for the purpose of this thesis. A typical discharge characteristic of a Li-Ion cell based on information available on Automotive Energy Supply Corporation's (A supplier of batteries for EV and Hybrid Electric Vehicles (HEV) applications) website [14] is as shown in the Fig. 1.3

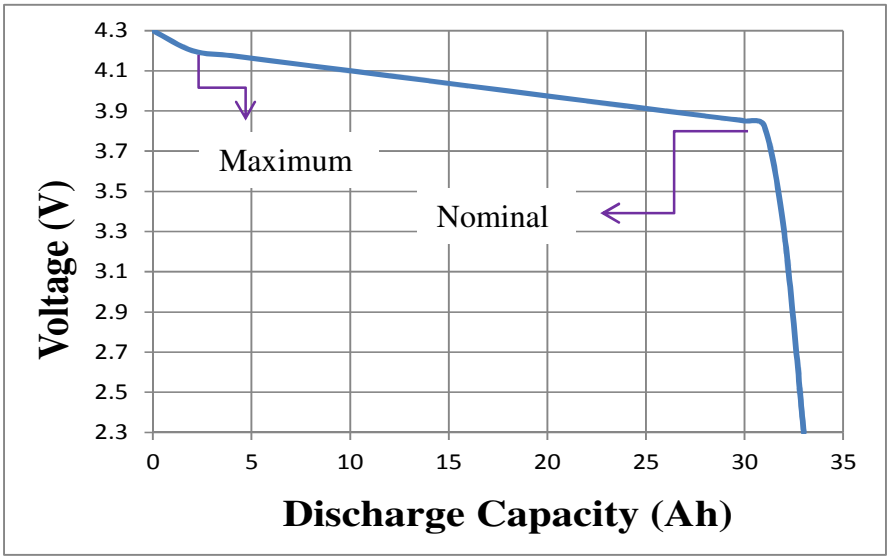

Fig. 1.3- Typical Discharge Characteristic of Li-Ion Battery Cell

Batteries can be discharged at different "C" rates. For example a 22 Ah battery, discharged at 1C will have a discharge current of 22 A and will take 1 hour to discharge completely. Whereas, if it is discharged at 0.33 C the discharge current will be 7.33 A and it will take 3 hour for the battery to discharge completely.

The Li-Ion battery used for the purpose of this thesis is assumed to have a battery pack with two cell modules connected in parallel and each rated for 33.1 Ah. Each of these cell modules contain 96 cells connected in series. Based on Fig 1.3 the maximum and nominal cell voltage for PEV battery is taken to be 4.2 V and 3.8 V, respectively. This gives battery capacity of 24 kWh as follows

$$Battery\,Capacity\left(kWh\right) = \frac{96 * 3.8 * 66.2}{1000} \cong 24$$

Fig. 1.4 shows the parameters fed in PSCAD™/EMTDC™ battery model for modeling PEV battery pack.

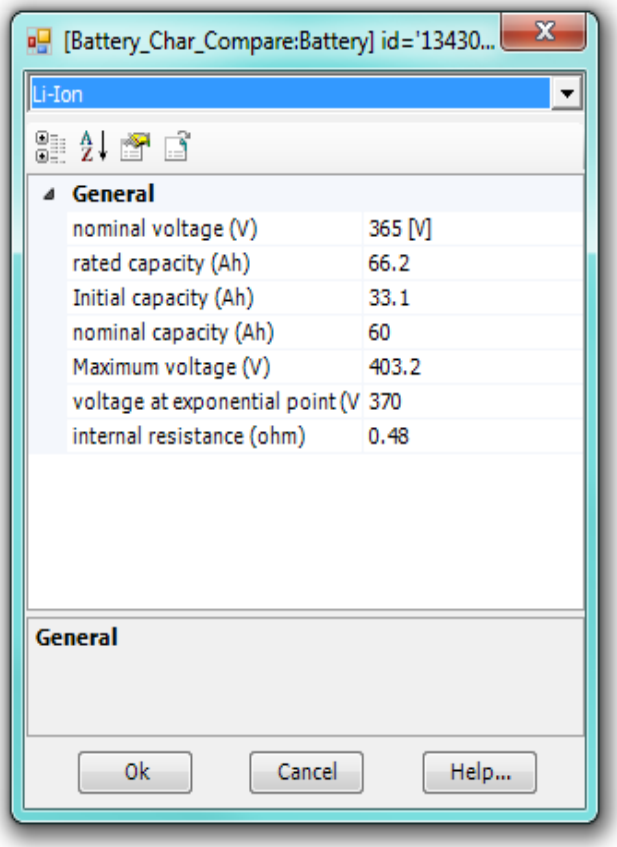

Fig. 1.4- Parameters for PEV Li-Ion Battery Pack

1.2.2 Modeling of Battery Chargers:

To study the impacts of PEVs on the distribution system, correct modeling of the battery charger is of utmost importance. The battery charger models developed for the purpose of this thesis is based on the information available in literature; details of which have been described as and when required. Two types of battery chargers with Voltage Source Converters (VSC) for AC/DC stage have been modeled. VSCs are inherently efficient, compact, and economical. They can be used for various functions that require minimum number of power conversions [15]. VSCs can be broadly classified as Current Controlled Voltage Source Converter (CCVSC) and Voltage Controlled Voltage Source

Converter (VCVSC). CCVSC directly controls the current flowing into VSC. This is achieved by generating switching signals based on error in input current with respect to the reference current value. In case of VCVSC, the magnitude and the angle of the converter side voltage with respect to grid side voltage phasor is controlled to obtain the desired power flow [15]. This chapter will describe CCVSC type of battery charging system while next chapter will go into details of modeling of VCVSC type of battery charging system. The two types of battery chargers have same topology and differ only in the control methodology applied to the AC/DC converter. This will help in comparing the similarities and difference in the impacts which the control methodologies of battery chargers may have on the distribution system. [6]

1.3 CCVSC type Battery Charger:

1.3.1 Topology and control of CCVSC type Battery Charger:

CCVSC type of the battery charger was modeled with two types of input filters. The topology of single phase, CCVSC type battery charger with L and LCL filter is as shown in Fig. 1.5 and Fig. 1.6. The cut-off frequency of 1.5 kHz is selected for LCL filter. Based on the information given in [16] and using (1.1), the value of the capacitor for the LCL filter is obtained to be 7.5×10^{-6} F. In order to avoid magnification of the frequency around the cutoff frequency, the value of the damping resistor in series with capacitor is chosen to be 0.5 ohm. [6]

$$Cutoff\ \ Frequency = \left(\frac{1}{2\pi}\right)\times\sqrt{\left(\frac{L_1 + L_2}{L_1 \times L_2 \times C}\right)} \qquad (1.1)$$

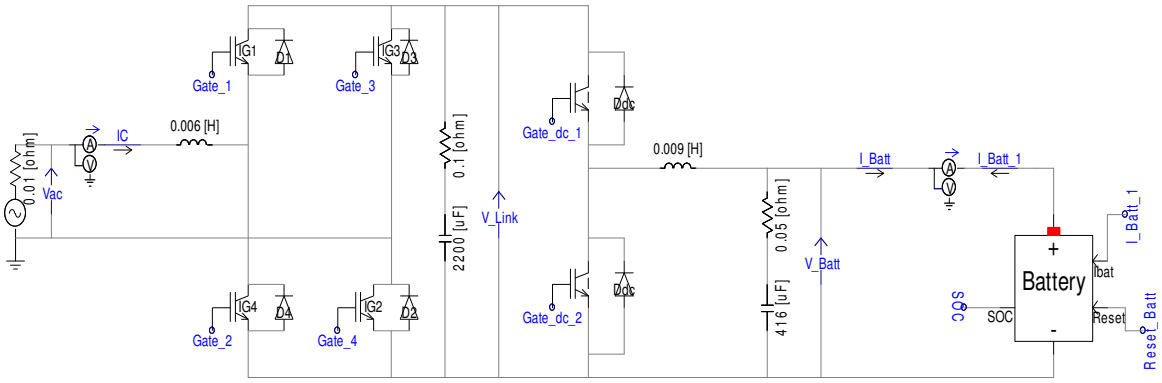

Fig. 1.5- Topology of Single Phase CCVSC Type Bidirectional Battery Charger with L Filter

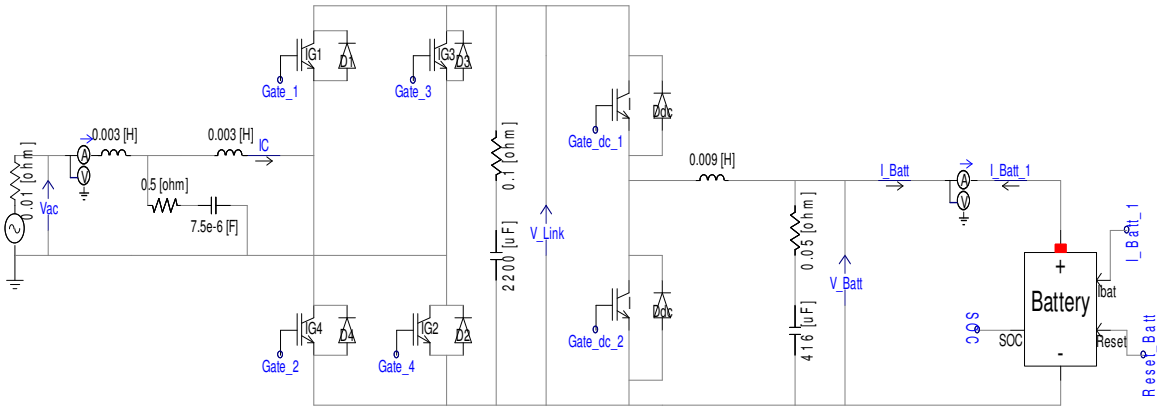

Fig. 1.6- Topology of Single Phase CCVSC Type Bidirectional Battery Charger with LCL Filter

The topology and the parameters of the charger are adopted from [5]. The value of the input inductor and DC/DC converter inductor were modified by observing the steady state and transient response of the charger [6]. The control of the charger is based on the methodology given in [12] and [17] and as described in [2]. The charger is capable of operating in all the four quadrants of the active-reactive power plane. However, for the purpose of this thesis, the charger is used and evaluated for its performance for unity power factor charging. The operation of the charger shown in Fig. 1.5 and Fig 1.6 can be divided in two stages: stage 1-AC/DC Converter Stage and stage 2-DC/DC Converter

Stage. The main aim of the AC/DC stage in unity power factor charging mode is to convert the AC input supply voltage to a DC voltage while ensuring that the input current taken is at unity power factor and the current harmonic distortion is low. The main aim of the DC/DC converter is to convert DC-Link voltage to required DC voltage based on the battery CC-CV charging algorithm. Thus AC/DC converter and DC/DC converter acts as a rectifier and buck converter respectively during charging mode and as an inverter and boost converter during discharging mode. [2]

The control for AC/DC converter stage is shown in Fig. 1.7 and Fig. 1.8

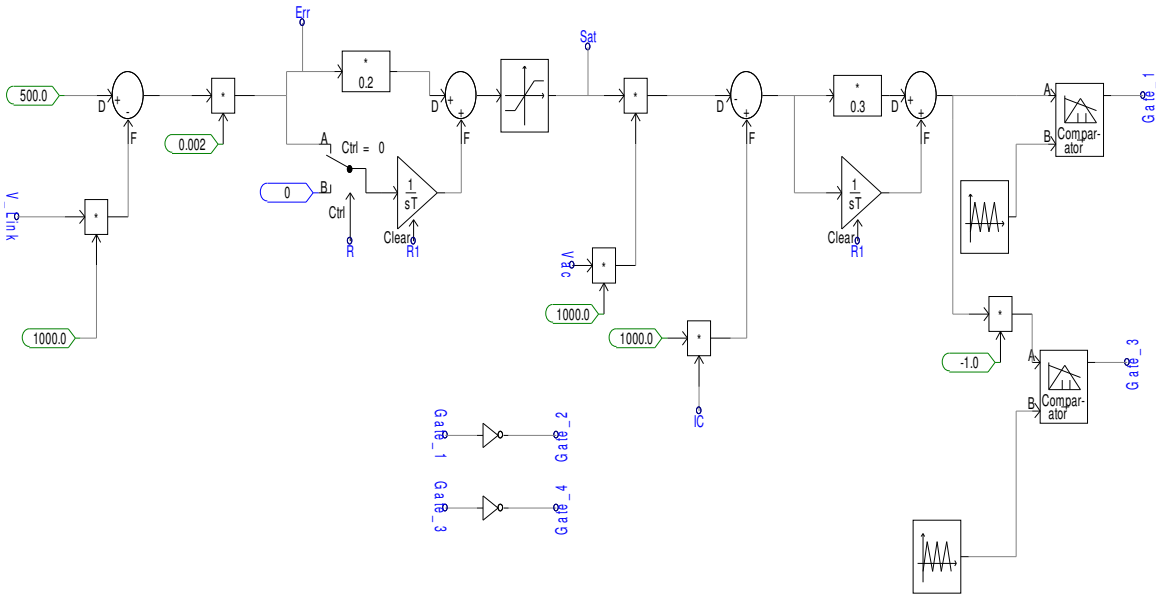

Fig. 1.7- Control for AC/DC Converter Stage For CCVSC Type Battery Charger

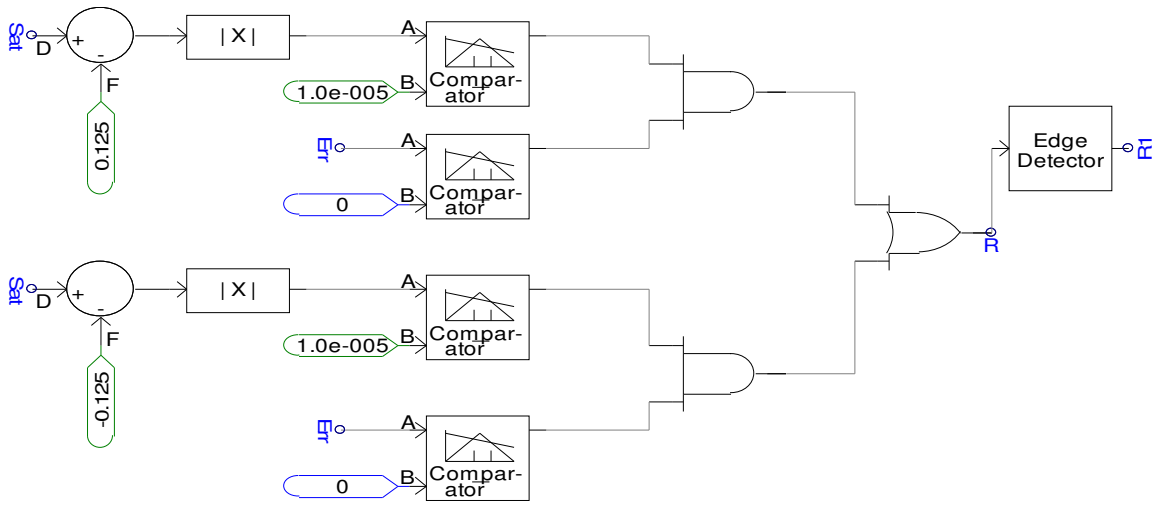

Fig. 1.8- Integrator Stop and Reset Logic For CCVSC Type Battery Charger

For the AC/DC converter stage in unity power factor charging mode, the reference DC Link voltage is compared with its actual value to generate the voltage error signal. This error signal is normalized and given to the first feedback proportional-integral (PI) controller. In order to obtain faster transient response, this PI controller is designed in such a way that whenever the output of the PI controller hits upper or lower limits defined by the saturation block and the error is in the same direction, the integrator stops integrating the error signal. When the output of the PI controller comes out of saturation, a reset signal is generated, which resets the integrators of all the PI controllers in the control system of the charger. The output of the first PI controller is the magnitude of the current demanded by the charger. This magnitude of current is then multiplied with the AC grid voltage to get the desired wave shape for the reference input current signal. This signal, when compared with actual value, generates a current error signal which is given to a second feedback PI controller. The output of the second PI controller generates gating signals for the AC/DC converter based on Sine Pulse Width Modulation (SPWM).

[2] Since the switching instants of the converter are determined by comparing the actual current flowing through the input inductor with the desired current, the control methodology is called CCVSC.

The controller for the DC/DC converter in charging mode is as shown in Fig. 1.9.

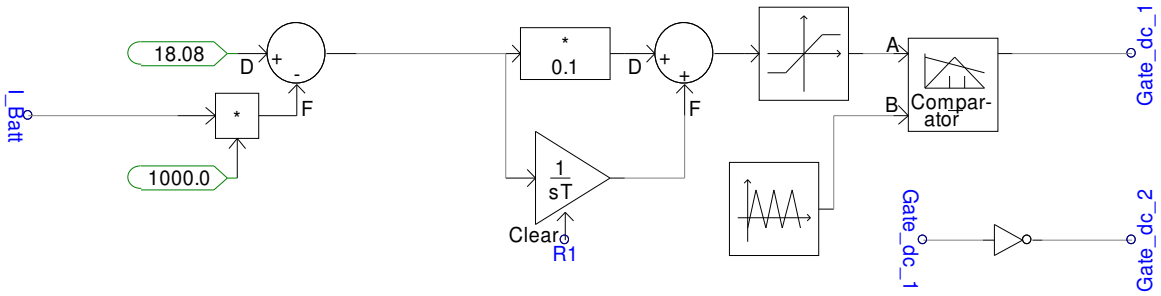

Fig.1.9- Control For DC/DC Stage For CCVSC Type Battery Charger

Since the SOC of the battery remains almost constant during the simulation time period, only CC charging is considered. The reference CC set point is compared with the actual value of the battery current to generate its error signal. This error signal is then given to the feedback PI controller to generate reference duty cycle for the DC/DC converter. The duty cycle is implemented by comparing reference duty cycle with high frequency triangular waveform generating appropriate gating signals for the switches. [2]

1.3.2 Steady State and Transient Response of CCVSC type Battery Charger:

A fault at the terminal of the charger was created at 2.5 s and cleared in 0.2 s. The steady state and transient response of CCVSC type battery charger with L filter and in unity power factor charging mode is as shown in the figures below

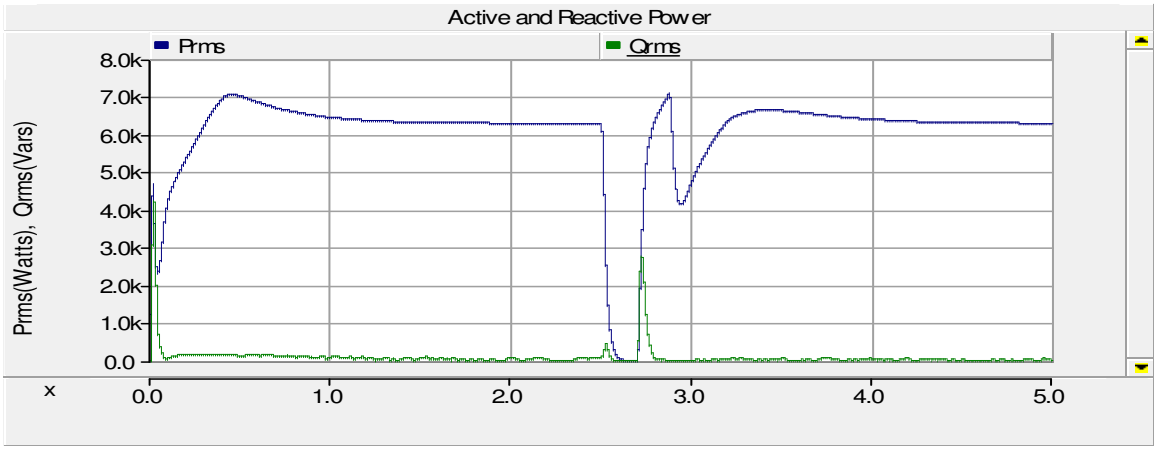

Fig.1.10- Active and Reactive Powers During Steady State And Transient Condition

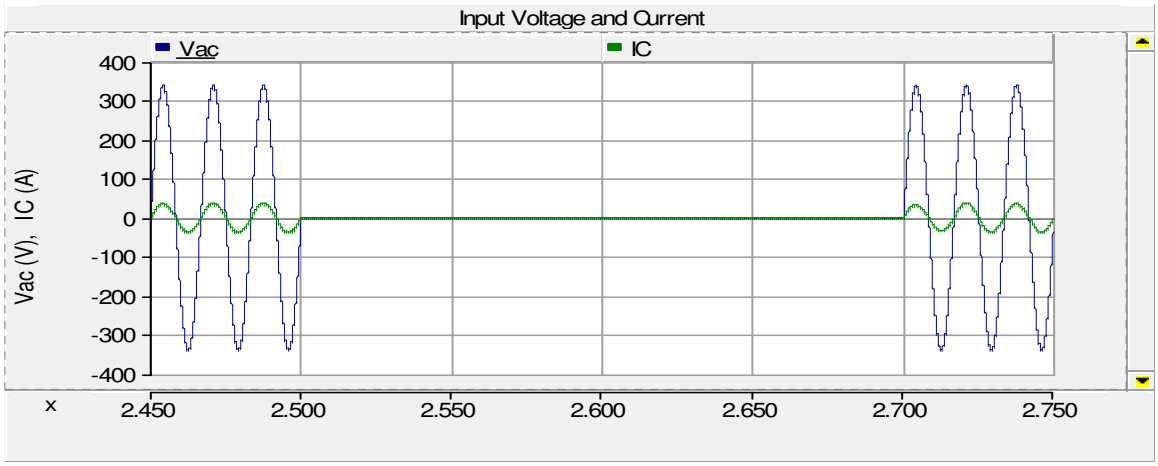

Fig.1.11- Input Current And Voltage During Steady Sate And Transient Condition

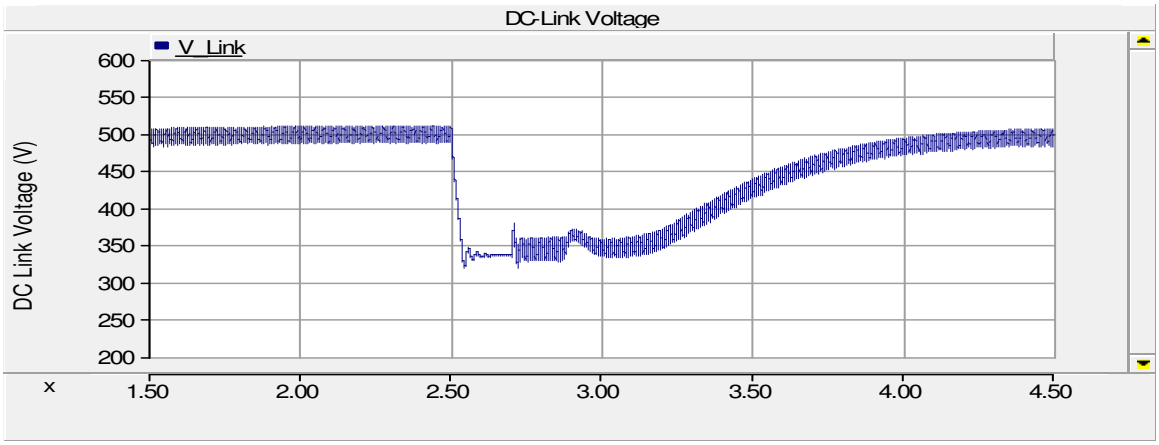

Fig.1.12- DC-Link Voltage During Steady Sate and Transient Condition

Table 1.2- Comparison: Active Power, Reactive Power and DC-Link Voltage

Quantity	Commanded Value	Actual Values (at 2s simulation time)
Active Power	6237.6 Watts	6303 Watts
Reactive Power	0 Vars	76 Vars
DC-Link Voltage	500 V	500 V (±10 V ripple Voltage)

The input current Total Harmonic Distortion (THD) was 4.34% and 3rd harmonic was found to be most dominant harmonic with its contribution being 2.72%

1.4 Summary:

This chapter provided introduction to PEVs and the infrastructure available to charge their batteries. The chapter also focused on describing the components involved in the battery charging system of a PEV and their functionality. It also explained in detail the charging requirements of Li-Ion batteries and modeling of the CCVSC type of battery charger. The chapter concluded by analyzing the performance of CCVSC type of battery charger in unity power factor charging mode.

CHAPTER TWO

VOLTAGE CONTROLLED VOLTAGE SOURCE CONVERTER TYPE OF BATTERY CHARGER

2.1 Control of VCVSC:

The last chapter described the modeling of CCVSC type of the battery charger in detail. This chapter deals with the VCVSC type of battery charger. The control of single phase VCVSC used for the battery charging system of PEVs has lot of parallelism with the control of Voltage Control Voltage Source Inverter (VCVSI) used in Distributed Energy Sources (DES) such as Photovoltaic (PV). The basic circuit and phasor diagram showing the flow of power between the grid and the converter is as shown in Fig 2.1.

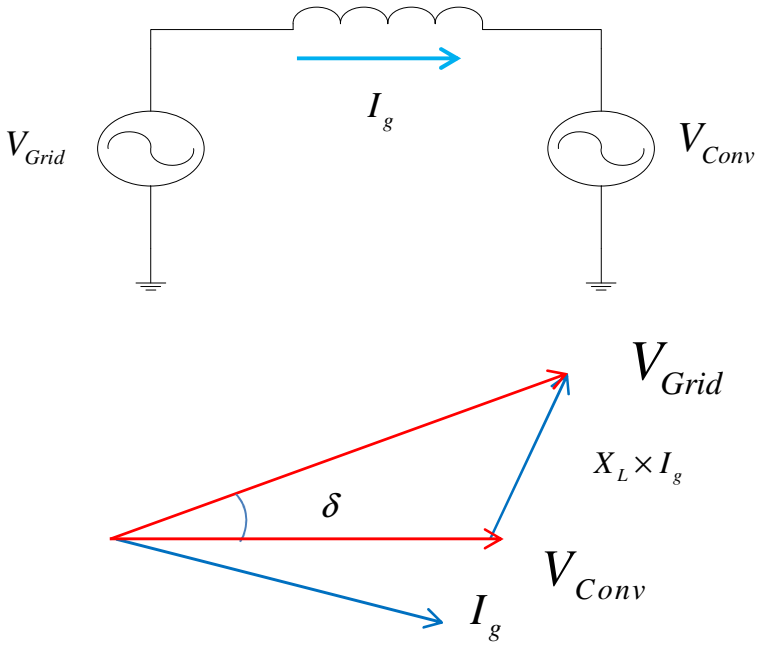

Fig. 2.1- Circuit and Phasor Diagram Relating Grid and Converter Voltage Phasor

The equations relating the flow of active and reactive power between grid and converter can be written as [18]

$$P = \frac{\left|V_{grid}\right| * \left|V_{conv}\right|}{X_L} * \sin(\delta) \tag{2.1}$$

$$Q = \frac{\left|V_{grid}\right|^2}{X_L} - \frac{\left[\left|V_{grid}\right| * \left|V_{conv}\right|\right]}{X_L} * \cos(\delta) \tag{2.2}$$

From equations 2.1 and 2.2 it can be seen that, by controlling the angle and magnitude of the converter side voltage with respect to grid side voltage phasor, flow of active and reactive power between grid and converter can be controlled. The angle and magnitude of converter side voltage can be controlled using direct or vector control methodology. The application and comparison of these methodologies used for control of power flow in High Voltage DC transmission has been described in [18]. Control of converter used in DES and PEVs can be described on the similar lines with the difference that the converter used for these applications are generally single phase

2.1.1 Direct Control of VCVSC:

In [19] the control of active and reactive power flow between the grid and PV is achieved by direct control methodology. The control scheme for direct control based on [19] is shown Fig. 2.2. The actual value of the active power flowing between the grid and PV is compared with the reference value to generate the power angle '**δ**'. In order to get the difference in the peak voltage 'ΔE' required between the grid and converter side voltage, the actual value of the reactive power flowing between the grid and PV is

compared with reference value. ‘δ’ and ‘ΔE’ thus obtained are then added to grid side voltage angle and maximum amplitude respectively to generate reference converter side voltage waveform. This waveform is then implemented using Pulse Width Modulation (PWM) techniques.

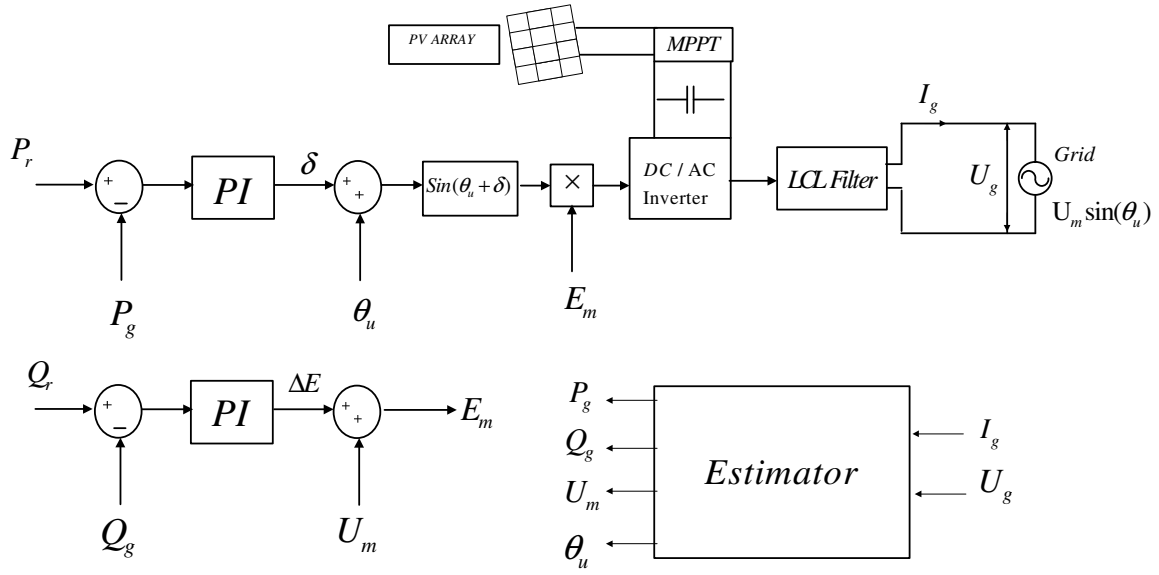

Fig. 2.2- Control Scheme for Direct Control Of VCVSC For PV [19]

One of the biggest disadvantages of the direct control method is that, the independent control of active and reactive power is not possible. This short coming can be solved by using vector control methodology.

2.1.2 Vector Control of VCVSC:

Due to its ability to control the active and reactive power independently, vector control of VCVSC is used for battery charging system in this thesis. The basic structure of the control methodology is based on [20] and [21] with all the necessary modifications incorporated to adapt it to PEV application which is as described in [6]. The topology of the vector controlled VCVSC type bidirectional battery charger with L and LCL filter is

same as CCVSC. The topology with LCL filter is as shown in Fig. 2.3 for ready reference. This charger is also capable of operating in all the four quadrant of P-Q plane, but for the purpose of this thesis it is used and evaluated for its performance for unity power factor charging.

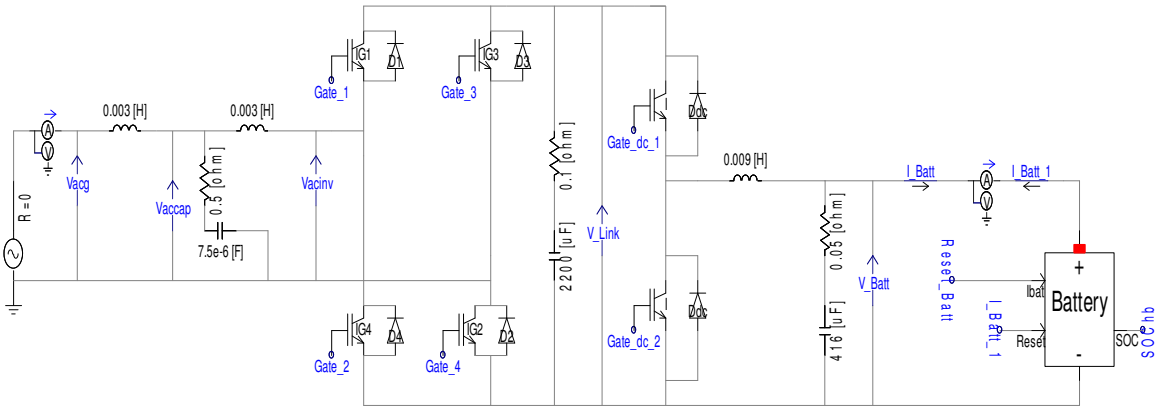

Fig. 2.3- Topology for VCVSC Type Bidirectional Battery Charger With LCL Filter

One of the very first steps in implementing the vector control is to obtain rotating space vectors for grid side voltage and current. In case of a three phase system, rotating space vectors are readily available, but same is not the case with single phase system. In single phase system a fictitious phase orthogonal to the original phase has to be created in order to obtain the rotating space vectors. Fictitious orthogonal phase can be created using various techniques such as 90° phase shift, Hilbert transformation, and Second Order Generalized Integrator (SOGI) [20]. In this thesis, SOGI is used to generate the fictitious orthogonal phase. The structure of SOGI used in the control of the battery charging system is shown in Fig. 2.4. [20][6]

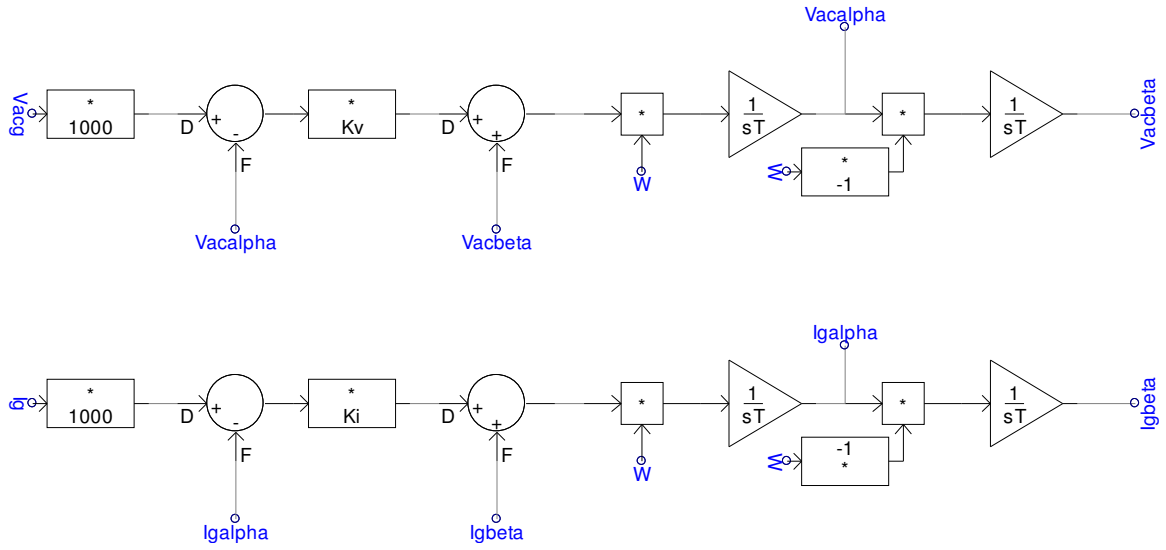

Fig. 2.4- Structure of Second Order Generalized Integrator

"V_{acg}" and "I_g" are the grid side voltage and current in kV and kA respectively. "$V_{acalpha}$" and "I_{galpha}" is the conditioned original phase voltage and current respectively. "V_{acbeta}" and "I_{gbeta}" is the fictitious orthogonal phase voltage and current respectively. "Kv" and "Ki" are the damping factors for voltage and current filters respectively and "W" is the base angular frequency. One of the main advantages of using SOGI for generation of fictitious orthogonal phase is its ability to filter the input voltage and current being fed to the control system [6] [22]. The filtering of the input voltage and current is dependent on selection of damping factors "Kv" and "Ki" respectively [22]. As the value of the damping factor decreases, the band pass becomes narrower resulting in heavy filtering. At same time the dynamic response of the system becomes slower [22]. For the purpose of this thesis Kv=1.4142 and Ki=0.6 were selected. The tuning of the SOGI is frequency dependent and hence problems could occur if it is tuned to nominal

frequency and there are fluctuations in grid frequency. In order to make the structure frequency adaptive, input "W " to the SOGI is dynamically fed from a Phase Locked Loop (PLL) [22]. The transfer function of the SOGI shown in Fig 2.4 is as given in equations 2.3 and 2.4 [20]

$$\frac{X_{\alpha}(s)}{X(s)} = \frac{(K_i \ or \ K_v) * W * s}{s^2 + (K_i \ or \ K_v) * W * s + W^2} \tag{2.3}$$

$$\frac{X_{\alpha}(s)}{X(s)} = \frac{-(K_i \ or \ K_v) * W^2}{s^2 + (K_i \ or \ K_v) * W * s + W^2} \tag{2.4}$$

The input and α-β phase values obtained as the output of SOGI for the grid side voltage and current are as given in the table 2.1 [6]

Table 2.1- α-β Axis Values for the Grid Side Voltage and Current

Input	**α**	**β**
$V_{acgmax}\sin(Wt)$	$V_{acgmax}\sin(Wt)$	$V_{acgmax}\cos(Wt)$
$I_{gmax}\sin(Wt-\emptyset)$	$I_{gmax}\sin(Wt-\emptyset)$	$I_{gmax}\cos(Wt-\emptyset)$

As mentioned before, the main aim of the vector control is to control the converter side voltage phasor based on desired value of active and reactive power flow. Once the rotating space vectors for the grid side voltage and currents are obtained the pseudo control algorithm to obtain converter side voltage phasor is as given below [6]

1) Synchronously rotating "d" axis is aligned with grid side voltage space vector and lagging "q" axis orthogonal to it

2) Components of the grid side current “Ig” along “d” and “q” axis is obtained. The “d” axis current is in phase with the voltage and hence controls the active power flowing between grid and the converter while “q” axis is in phase quadrature and hence controls the reactive power

3) For a given state of charge, the battery voltage is almost constant. In constant current charging mode, the current flowing in to the battery is regulated by DC/DC converter. Hence active power is basically controlled by DC/DC converter. However, changes in active power flow are reflected as changes in DC-Link voltage which is desired to be maintained at a constant value. Hence, DC-Link voltage can be used to control the flow of active power. The error in the DC-Link voltage with respect to its reference value is used to generate the reference value for “d” axis current

4) The error in reactive power with respect to the commanded reference value is used to generate reference value of “q” axis current

5) Errors in “d” and “q” axis currents, based on the actual and reference values obtained from steps 2, 3, and 4, is used to generate converter side “d” and “q” axis voltages.

6) Converter side “d” and “q” axis voltage are transformed back to “α” and “β” axis. “β” axis being a fictitious axis is discarded. The “α” axis converter side voltage is the desired voltage which is implemented using SPWM.

The implementation of the vector control of VCVSC type of battery charger based on the pseudo algorithm is explained in detail.

In order to generate the rotating space vector for the grid side voltage and current with same frequency and direction of rotation as the grid side voltage phasor, the "α-β" axis are assumed to be located in space as shown in Fig. 2.5 [6]

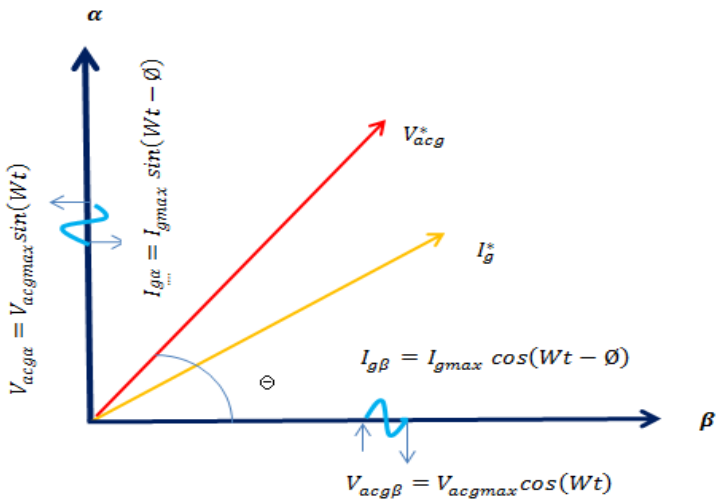

Fig. 2.5- Generation of Rotating Space Vectors For Grid Side Voltage and Current

"V^*_{acg}" and "I^*_g" are the space vectors for grid side voltage and current respectively. Once the rotating space vectors for grid side voltage and current are obtained, the synchronously rotating "d" axis is aligned with grid side voltage space vector and "q" axis orthogonal to it. With this alignment the component of the grid side voltage along the "q" axis is zero. In order to appropriately align the "d" axis the value of "θ" should be known at all time. This is achieved by using a PLL for grid side voltage phasor. The PLL used for the purpose of this thesis is as described in [22] and is shown in Fig 2.6 where "ThV_{ac}" = θ

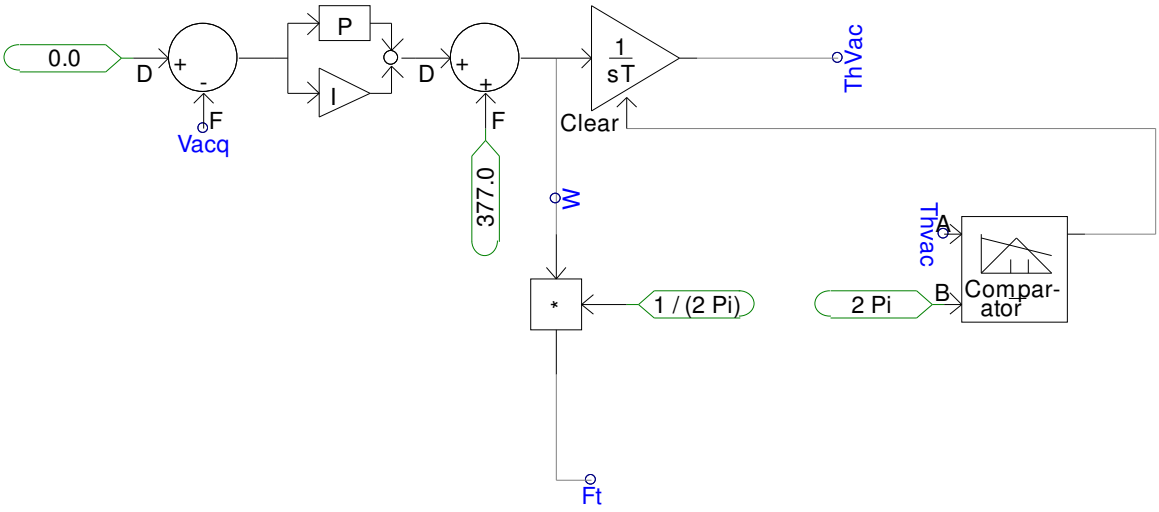

Fig. 2.6- PLL For Grid Side Voltage Phasor

Since the component of the grid side voltage along the "q" axis should be zero, is it used as the feedback to track the grid side voltage phasor and hence for generation of angle "θ ". Since the PLL dynamically track the angular frequency of grid side voltage phasor, its output is used in SOGI shown in Fig. 2.4 to make it adaptive to frequency variations.

Once angle "θ " is obtained from the PLL mentioned above, the grid side voltage and current space vectors are transformed to "d" and "q" axis using the transformation matrix as shown in equation 2.5 and 2.6. The graphically representation of the transformation is as shown in Fig. 2.7

$$\begin{bmatrix} V_{acd} \\ V_{acq} \end{bmatrix} = \begin{bmatrix} \sin(\theta) & \cos(\theta) \\ -\cos(\theta) & \sin(\theta) \end{bmatrix} \begin{bmatrix} V_{ac\alpha} \\ V_{ac\beta} \end{bmatrix} \tag{2.5}$$

$$\begin{bmatrix} I_{gd} \\ I_{gq} \end{bmatrix} = \begin{bmatrix} \sin(\theta) & \cos(\theta) \\ -\cos(\theta) & \sin(\theta) \end{bmatrix} \begin{bmatrix} I_{g\alpha} \\ I_{g\beta} \end{bmatrix} \tag{2.6}$$

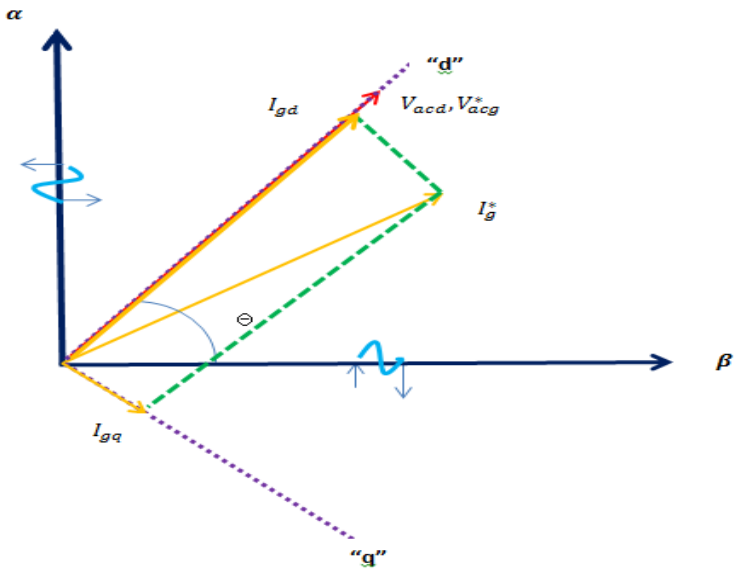

Fig. 2.7- Mapping of Grid Side Voltage and Current On "d-q" Axis

The reference value for the "d" axis current is obtained from the error in DC-Link voltage which in turn is linked to the active power commanded by the charger. The difference in actual and commanded reactive power is used to generate the reference value for the "q" axis current. Applying Kirchhoff's Voltage law (KVL) for the loop between grid side voltage "V_{acg}" and converter side voltage "V_{acinv}" indicated in Fig 2.3 and neglecting the filtering capacitor, we get equation 2.7.

$$V_{acg} = L\frac{d}{dt} I_g + V_{acinv} \tag{2.7}$$

The transformation matrix used in equation 2.5 and 2.6 and its inverse can be defined as

$$T = \begin{bmatrix} \sin(\theta) & \cos(\theta) \\ -\cos(\theta) & \sin(\theta) \end{bmatrix} \qquad T^{-1} = \begin{bmatrix} \sin(\theta) & -\cos(\theta) \\ \cos(\theta) & \sin(\theta) \end{bmatrix} \tag{2.8}$$

Writing equation 2.7 in "α-β" domain we get

$$\begin{bmatrix} V_{ac\alpha} \\ V_{ac\beta} \end{bmatrix} = L \frac{d}{dt} \begin{bmatrix} I_{g\alpha} \\ I_{g\beta} \end{bmatrix} + \begin{bmatrix} V_{acinv\alpha} \\ V_{acinv\beta} \end{bmatrix} \tag{2.9}$$

Transforming equation 2.9 from "α-β" to "d-q" domain using equation 2.8 we get

$$T^{-1} \begin{bmatrix} V_{acd} \\ V_{acq} \end{bmatrix} = L \frac{d}{dt} T^{-1} \begin{bmatrix} I_{gd} \\ I_{gq} \end{bmatrix} + T^{-1} \begin{bmatrix} V_{acinvd} \\ V_{acinvq} \end{bmatrix} \tag{2.10}$$

Pre- multiplying equation 2.10 by "T" we get

$$\begin{bmatrix} V_{acd} \\ V_{acq} \end{bmatrix} = T\ L \frac{d}{dt} T^{-1} \begin{bmatrix} I_{gd} \\ I_{gq} \end{bmatrix} + \begin{bmatrix} V_{acinvd} \\ V_{acinvq} \end{bmatrix} \tag{2.11}$$

On simplifying equation 2.11 we get the final form of the equation as given in equation 2.12 and 2.13

$$\begin{bmatrix} V_{acd} \\ V_{acq} \end{bmatrix} = L \frac{d}{dt} \begin{bmatrix} I_{gd} \\ I_{gq} \end{bmatrix} + \begin{bmatrix} 0 & \omega L \\ -\omega L & 0 \end{bmatrix} \begin{bmatrix} I_{gd} \\ I_{gq} \end{bmatrix} + \begin{bmatrix} V_{acinvd} \\ V_{acinvq} \end{bmatrix} \tag{2.12}$$

$$\begin{bmatrix} V_{acd} \\ V_{acq} \end{bmatrix} = V_L + \begin{bmatrix} 0 & \omega L \\ -\omega L & 0 \end{bmatrix} \begin{bmatrix} I_{gd} \\ I_{gq} \end{bmatrix} + \begin{bmatrix} V_{acinvd} \\ V_{acinvq} \end{bmatrix} \tag{2.13}$$

The converter side "d" and "q" axis voltages can be expressed in terms of grid side "d" and "q" axis voltages based on 2.13 as follows

$$V_{acinvd} = V_{acd} - V_L - \omega L * \mathrm{I}_{gq} \tag{2.14}$$

$$V_{acinvq} = V_{acq} - V_L + \omega L * \mathrm{I}_{gd} \tag{2.15}$$

Equation 2.14 and 2.15 gives the relation between the grid and converter side volatge in d-q reference frame. The decoupled "d-q" axis circuit based on equations 2.14 and 2.15 is as shown in Fig. 2.8 [6]

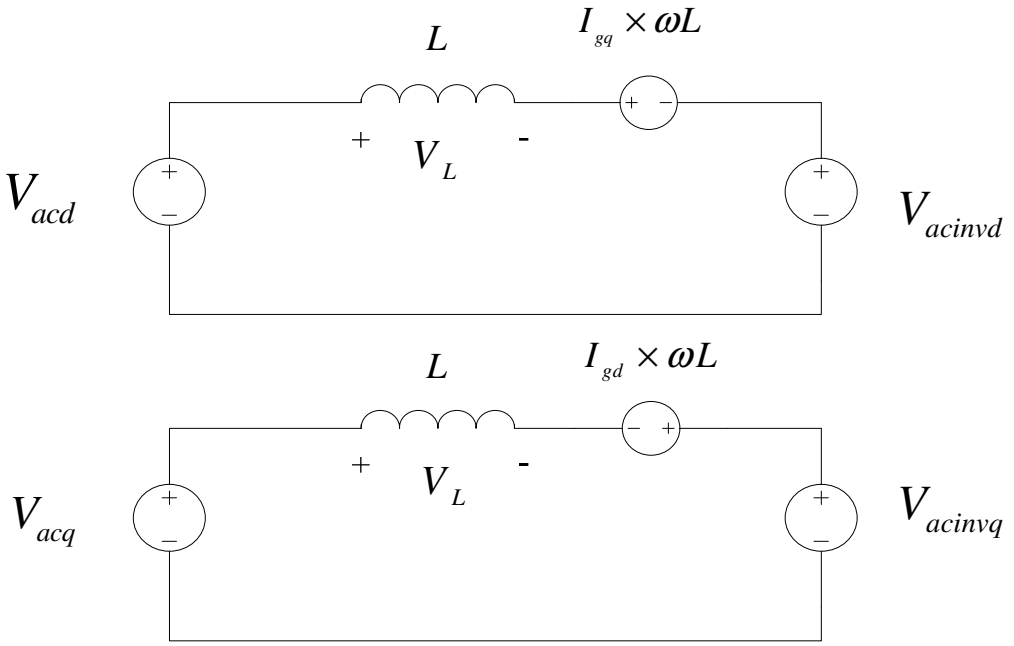

Fig. 2.8- Decoupled "d-q" Axis Circuit Relating Grid and Converter Side Voltages

The control circuit implemented in PSCAD™/EMTDC™ to obtain the converter side "d" and "q" axis voltages is as shown in Fig. 2.9 and 2.10 respectively [6]

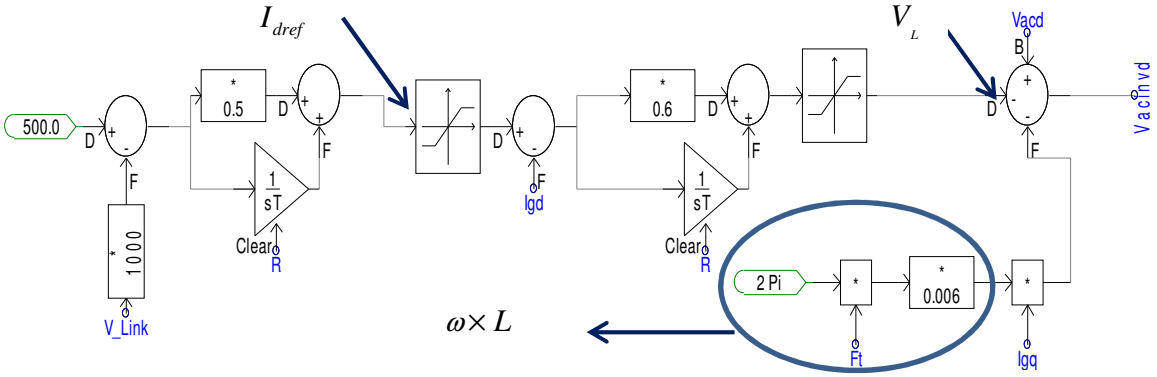

Fig. 2.9- Control Circuit To Obtain Converter Side "d" Axis Voltage

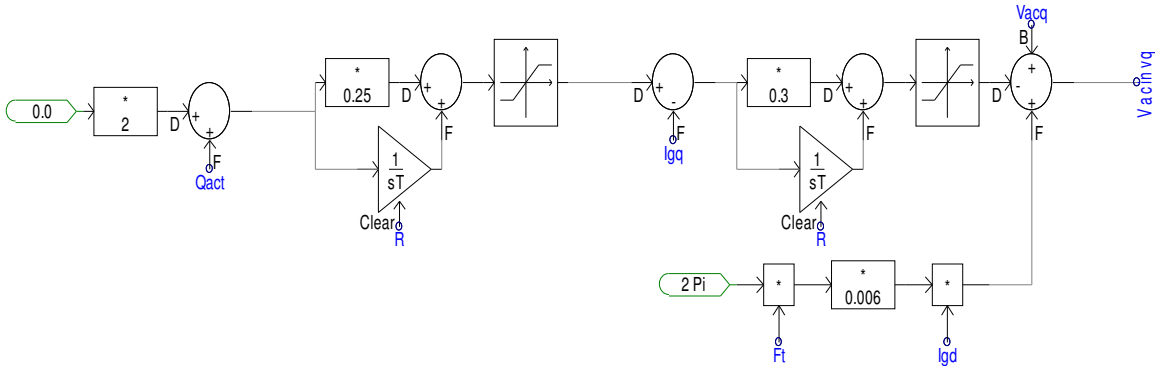

Fig. 2.10- Control Circuit to Obtain Converter Side "q" Axis Voltage

The converter side "d" and "q" axis voltages are transferred back to "α-β" domain using the inverse of the transformation matrix "T^{-1}" as defined in equation (2.8). The converter side "β" axis voltage is discarded as it is a fictitious phase and the "α" axis voltage thus obtained is implemented using SPWM.

2.1.3 Steady State and Transient Response of VCVSC type Battery Charger:

A fault at the terminal of the charger was created at 4 s and cleared in 0.2 s. The waveforms of the various quantities during steady state and transient conditions are as shown in the figures below. Whenever the voltage dips below 200 V at the terminals of the charger, after a delay of 1s, a reset command is generated for all the integrators in the control circuit of the charger. It is done to clear the control circuit of the accumulated errors during the operation of the charger in transient condition.

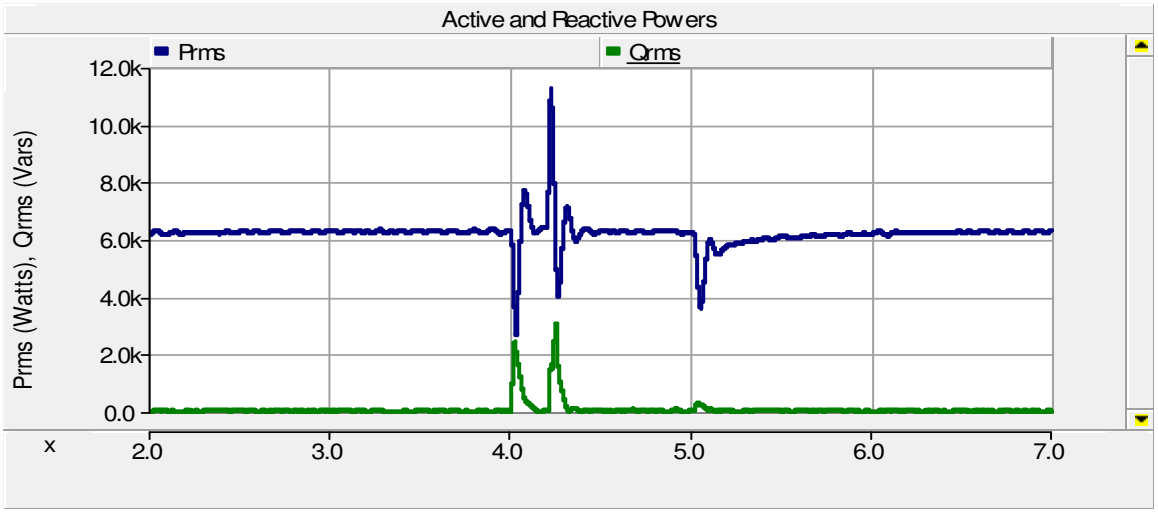

Fig. 2.11- Active and Reactive Power during Steady State and Transient Condition

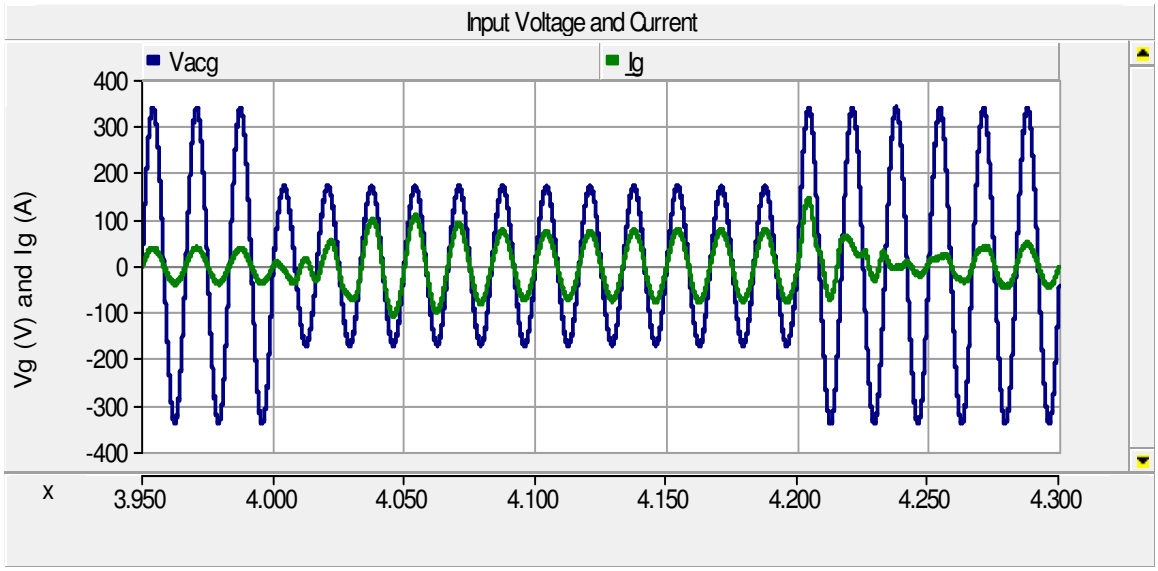

Fig. 2.12- Input Current and Voltage during Steady Sate And Transient Condition

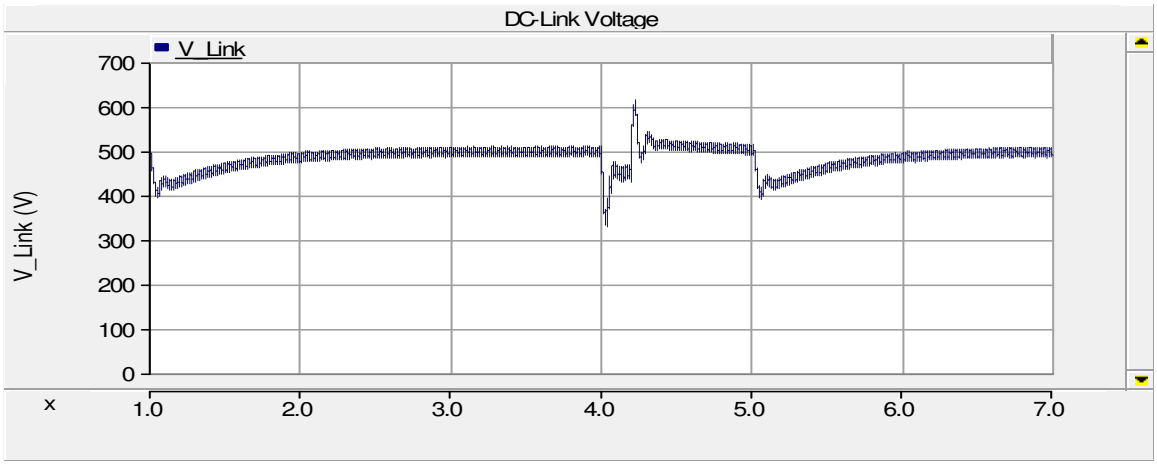

Fig. 2.13- DC-Link Voltage During Steady Sate And Transient Condition

Table 2.2 shows the steady state quantities commanded by the charger and their actual values

Table 2.2- Comparison of Commanded Active Power, Reactive Power and DC-Link Voltage with Their Actual Values

Quantity	Commanded Value	Actual Values (at 3s simulation time)
Active Power	6237.6 Watts	6295 Watts
Reactive Power	0 Vars	25 Vars
DC-Link Voltage	500 V	500 V (±10 V ripple Voltage)

The input current (THD) was 1.16% and none of the lower order harmonics were found to be dominant.

DC/DC converter control for VCVSC type of battery charger is similar to CCVSC type and has been described in details in Chapter 1

2.3 Development of Average Value Model:

In the battery charger described above, a PWM switching frequency of 3 kHz is used for both AC/DC and DC/DC converter. In typical Electro Magnetic Transient Program (EMTP) software, which utilizes a fixed time step, change in topology of the system due to switching of the power electronic devices requires special consideration [23]. This is because of the possibility of change in topology occurring within a given time step for which solution is being calculated. If the EMPT algorithm detects that a change in topology has occurred in between a given time steps, the solution for the nodal equations obtained at the end of the time step are discarded and a special routine of the algorithm is called for. The routine solves nodal equations using smaller time steps till the point where switching has occurred and topology has changed. The network topology is then updated and the final solution for the nodal equations is obtained with the modified topology [23]. Higher switching frequency of multiple power electronic devices lead to heavy computational burden and simulation time increases considerably.

One of the ways to circumvent this problem is to use Circuit Average Value Model (CAVM). In CAVM the linear components of the circuit such as inductors, capacitors etc. are kept as it is. The switching device circuitry is replaced by the controlled voltage and current sources in a manner that the terminal conditions are satisfied at all the instances. The topology of the CAVM is as shown in the Fig. 2.14

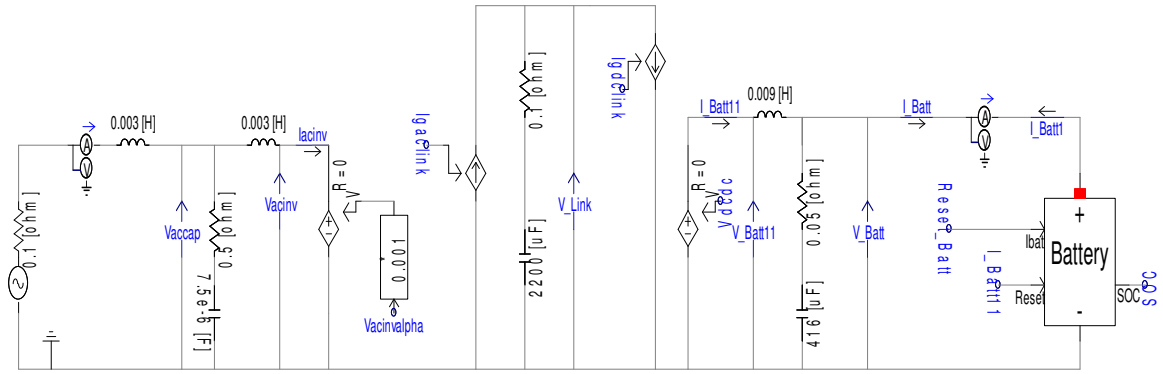

Fig. 2.14- Topology of Circuit Average Value Model for VCVSC

The control for generation of the converter side reference voltage signal is exactly same as in case of detailed model. The difference between the detailed model and the CAVM is that, in case of the detailed model the reference voltage signal is implemented by generating the desired gating signals using SPWM technique, whereas in CAVM it is implemented using a controllable voltage source. In the case of the detailed model, the control for the DC/DC converter generates the duty cycle value for the converter based on the desired current flow required to the battery. This value is then compared with high frequency triangular waveform in order to generate the gating signals required to obtain desired voltage modulation. In case of CAVM, the duty cycle value generated by the control is multiplied by the instantaneous DC link voltage. The resultant signal is then applied to a controlled voltage source to replicate the effect of voltage modulation. The duty cycle generated by the control is hard limited within the band zero to one. This is because, is case of detailed model, the duty cycle above one simply mean that switch is always closed and the DC-Link voltage at that instant is continuously being applied at the other side of the converter. However, in the case of CAVM, since duty cycle is being multiplied with the DC-Link voltage, duty cycle higher than one will result in application

of higher than the actual DC-Link voltage to the controlled voltage source. This will lead to violation of the terminal conditions with respect to the detailed model.

If we do not take in to account the losses taking place in the converters, the power on the left side of the DC-Link will equal to the product of converter side voltage and current. Similarly, the power on the right side of the DC-Link will be equal to the product battery side voltage and current before the filter. Based on the power balance, the value for the controlled current sources in the DC-Link circuitry of Fig. 2.14 can be determined by dividing the powers by the instantaneous DC-Link voltage. Based on Fig. 2.14, determination of input values for controlled current sources is as shown in Fig. 2.15

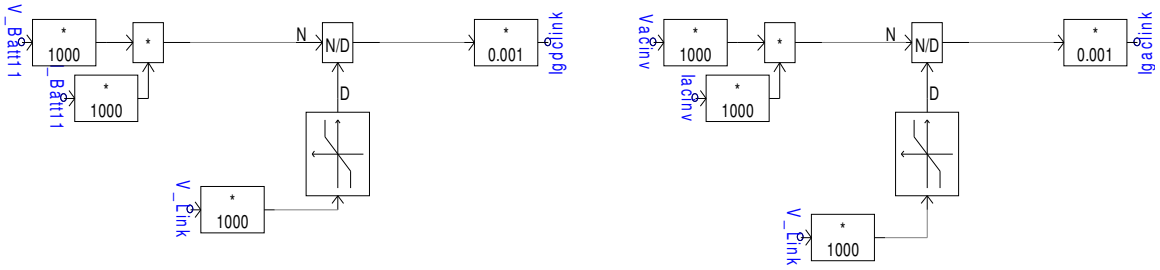

Fig. 2.15- Determination of Controlled Current Source Signals For CAVM

Since determination of the signals for controlled current sources require division by DC-Link volatge, its lower end value in the control is hard limited to one.

2.3.1 Comparison of Detailed and Average Value Model:

The comparison of various quantities for the detailed and the average value model during steady sate and the transient conditions for unity power factor charging is as shown in figures below. A fault at the terminal of the charger was created at 1s and cleared in 0.2 s.

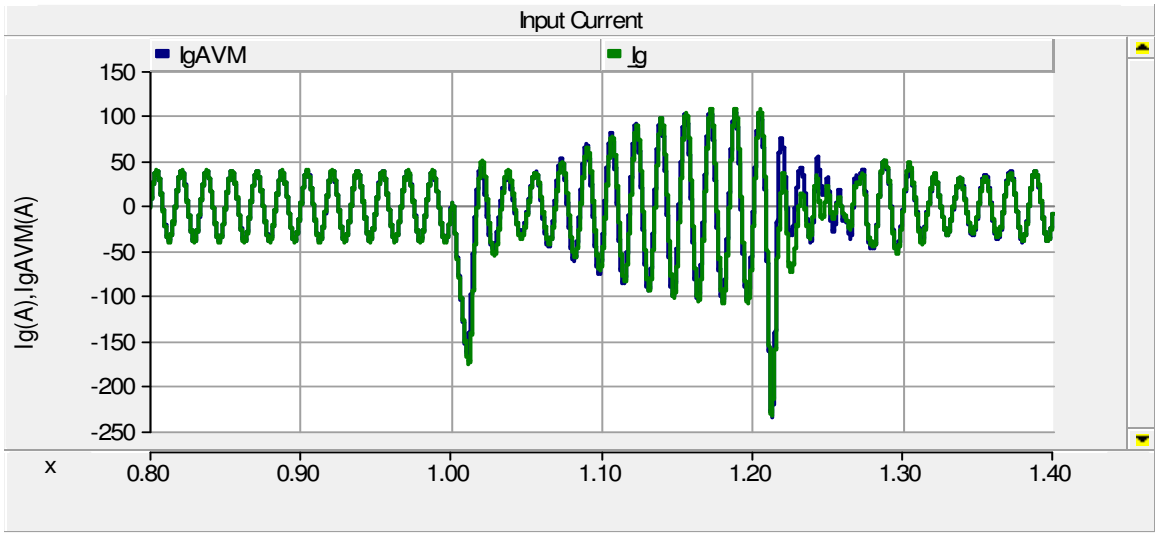

Fig. 2.16- Input Current For The Detailed and Average Value Model

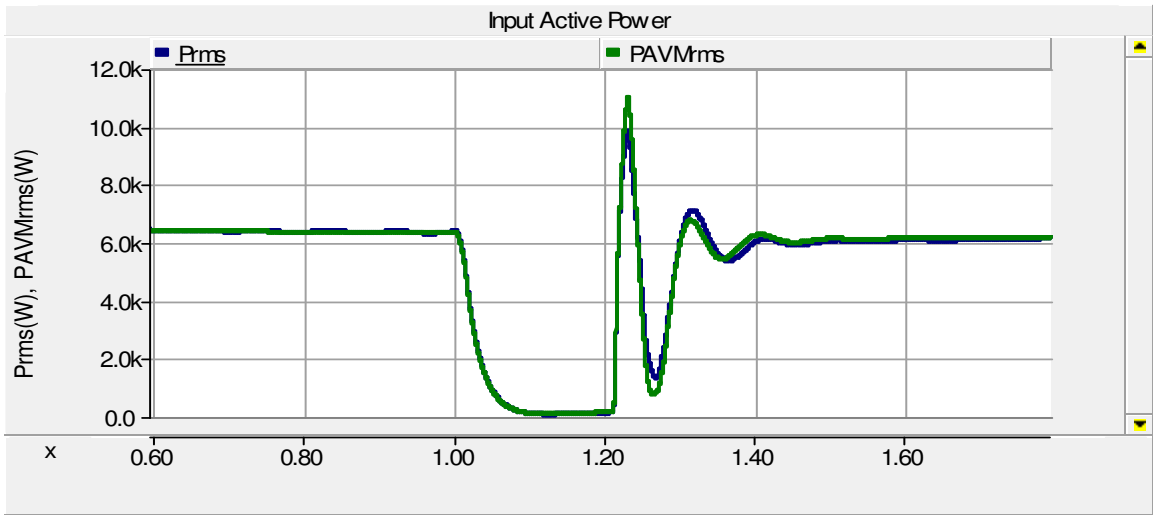

Fig. 2.17- Input Active Power For the Detailed And Average Value Model

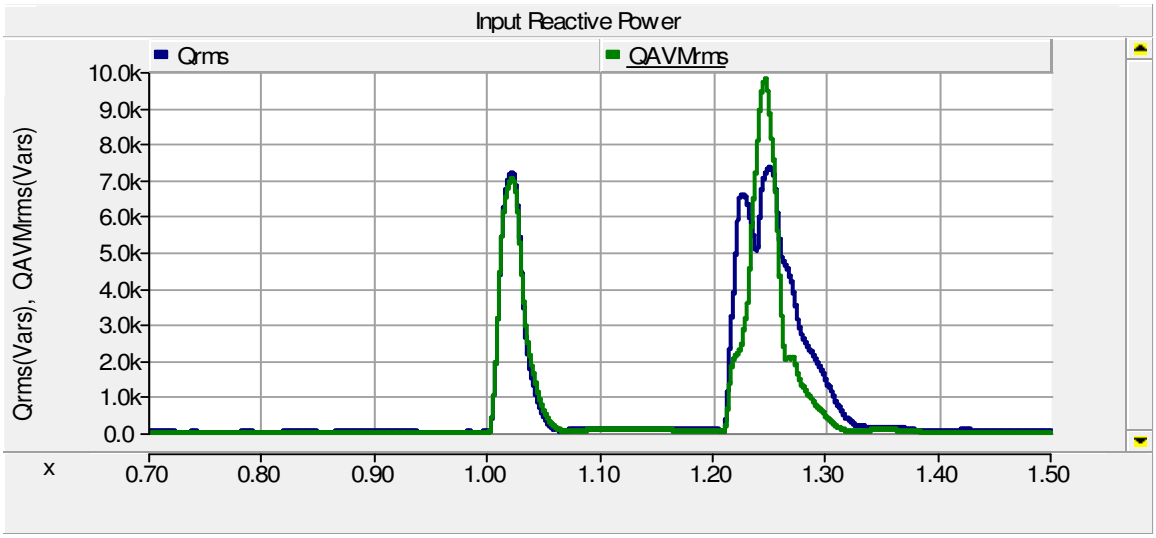

Fig. 2.18- Input Reactive Power For The Detailed And Average Value Model

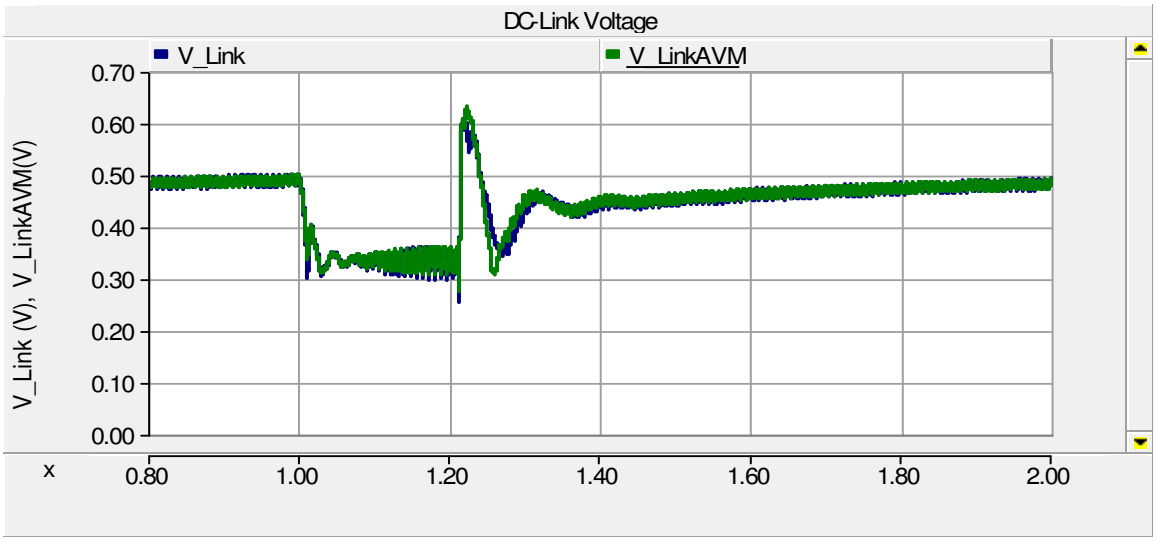

Fig. 2.19- DC-Link Voltage for The Detailed And Average Value Model

As can be seen from the figures above, the steady state as well as the transient response of the CAVM and the detailed model of the battery charging system, for unity power factor charging matches very closely. The reactive power taken by the two tpes of model are not in total confirmity with each other duirng the fault. However, looking at the

waveforms of other quantity it can be said that reactive power does not impact the performance of CAMV to a great extent. The performance of CAVM for other modes of operation has not been evaluated. The usage of the CAVM for the battery charger reduces the simulation time drastically. For IEEE 13 bus test distribution system, with 16 vehicles connected to each of the three phases at one of the bus in the system, usage of CAVM in repalcement of detailed model led to reducion in simulation time by approximately 67%

2.4 Summary:

This chapter focuses on describing VCVSC type of battery charger. An overview of Direct Control and Vector Control methodology is presented and the later is described in detail. The steady state and the transient performance of the VCVSC type of the battery charger is evaluated for unity power factor charging mode and is found to be satisfactory. In order to reduce simulation time, a CAVM for the VCVSC type of battery charger is developed. The steady state and the transient response of the detailed model and CAVM for unity power factor charrging mode are compared and it is concluded that they match very closely.

CHAPTER 3

IMPACTS OF PLUG-IN ELECTRIC VEHICLES ON DISTRIBUTION SYSTEM

3.1 Introduction:

Last couple of chapters described the modeling of CCVSC and VCVSC type of battery charging system for the PEVs. The main aim of this thesis is to study the impacts which the battery charging system of the PEVs will have on the distribution system. Considerable amount of research has already been done in order to study the impacts of PEVs on the electric grid and concocting methodologies to alleviate them. In [24], the aggregated load profile of PHEVs based on the data from National Household Travel Survey (NHTS), All Electric Range (AER) of PHEVs and its charging level is analyzed. Based on the analysis, different smart charging policies are suggested to shift the peak of the load profile to a desirable time of the day [6]. Research has also focused on studying the impact of PEVs on the assets of the of the distribution system. Distribution transformer is considered one of the most critical assets in distribution system. Estimating the remaining life of transformer is useful for reliability and planning of the system. Aging of transformer is mainly associated with degradation of its insulation, which is very sensitive to the temperature. In [25] the hot spot temperature in the transformer is estimated using NHTS data and IEEE standard dynamic thermal model. The study concludes that, with PEVs in the system, ambient temperature plays a critical role in accelerated aging of transformer and that some of the proposed smart charging algorithm may actually have adverse effect on its life. It also suggests a smart charging algorithm based on transformer temperature to mitigate the adverse effects of PEVs [6]. Research

in the domain of PEVs has also concentrated on developing smart charging algorithms to minimize losses and investment costs in distribution system [26], [27] and to optimally utilize PEVs for regulation and ancillary services [28], [29].[6]

Faults on a distribution system are a common phenomenon and the probability of it being a SLG fault is the highest. Very little work has been done in terms of analyzing the impacts which PEVs in a smart car park may have on the system during faults. In this thesis a smart car park of PEVs in an IEEE 13 Node Test Feeder is simulated. A SLG fault with auto-reclosure operation is created and response of the smart car park, in terms of impacts on system voltages, currents and power flows is analyzed. [6]

Photovoltaic (PVs) power is becoming less expensive and its growth is expected to be much greater in the near future [30]. In order to study the interaction between the PEVs and the PVs during the fault on the system, the studies are repeated with high penetration of the PVs in IEEE 13 Node Test Feeder.

3.2 Impacts of PEVs on Distribution System without PV Penetration:

3.2.1 System Description:

The IEEE 13 Node Test Feeder [31] as shown in Fig. 3.1 is used for this research. This primarily 4.16 kV distribution test system consists of 13 buses and 10 lines and cables. Of the thirteen buses, eight are three phase, three are two phase, and two are single phase [31]. Due to the small time step required for the simulation and the short lines present in the system, all distribution lines are modeled using mutually coupled lines. The mutually coupled line model neglects line capacitance and allows for less line detail, however it provides for a much faster simulation by allowing for a larger solution

time step [6]. In order to validate this model, a comparison of the system using the full detailed model of the distribution lines as found in [32] and the system using the mutually coupled lines is performed. The result of the comparison can be found in Fig. 3.2. From the plot it can be concluded that there is almost no appreciable difference between the two models for the purposes of this research [2].

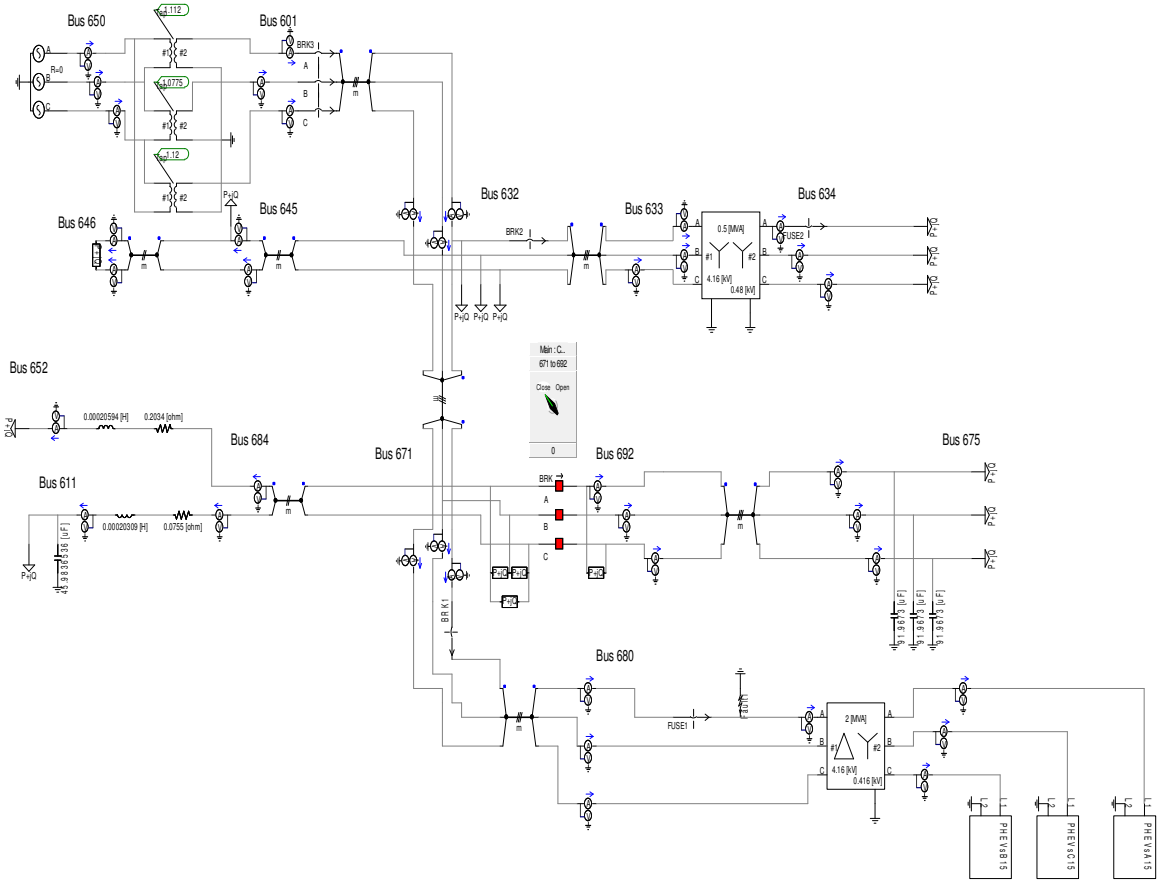

Fig. 3.1- IEEE 13 Node Test Feeder with PEVs in the System

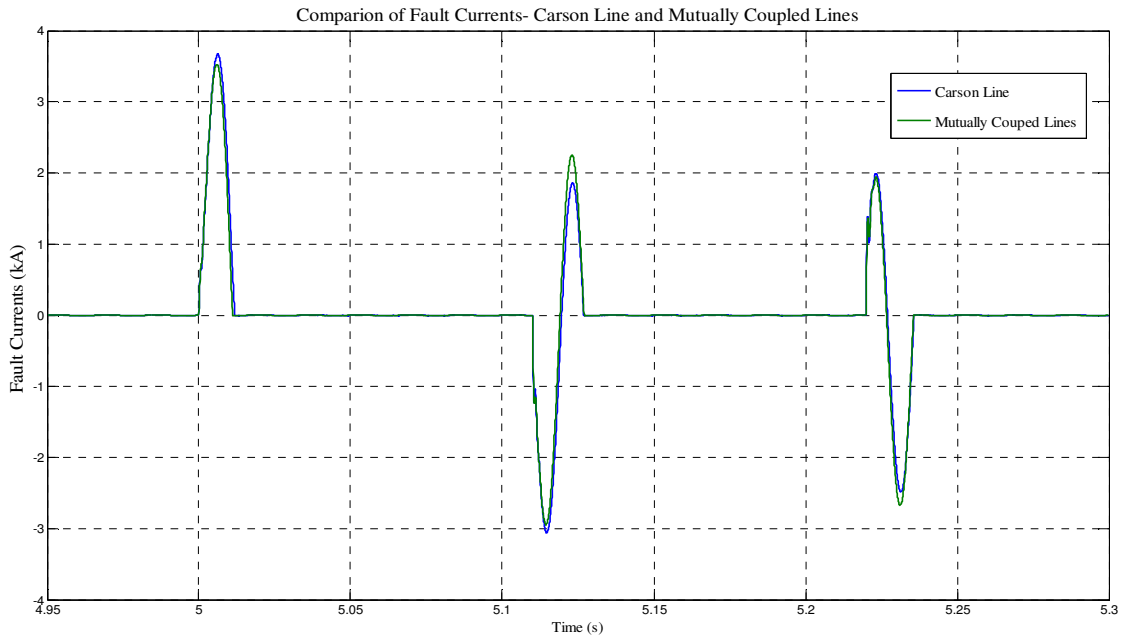

Fig. 3.2- Comparison of Fault Currents using Carson Lines and Mutually Coupled Line

In order to determine the effect the penetration of PEVs has on a distribution system, a 416 V bus is added to the system for the connection of PEVs. This bus is connected to the IEEE 13 Node Test Feeder through a Delta-Wye Grounded connected transformer attached to bus 680. On each phase of the secondary, sixteen PEV chargers are connected in parallel. Each vehicle draws approximately 6.2 kW of power during charging, for a total additional load of 99.2 kW per phase above the base system. A single phase recloser with the opening and closing timings found in Table 3.1 is added to phase A of the line connecting bus 671 to bus 680. [6]

Table 3.1- Recloser Timings

Cycle Type	Open Time	Close Time
Fast	0.1 Second	0.01 Second
Slow	0.1 Second	0.5 Second

A temporary SLG fault is applied to phase A of bus 680. The fault is applied 5 seconds into the simulation in order to allow the system to initialize and settle into steady state and it is cleared after duration of 0.275 seconds. The fault is cleared when single phase reclosure of the line connecting buses 671 and 680 is still open, disconnecting phase A of bus 680 from the main system. In order to isolate the impact of adding vehicles to the distribution system at bus 680 from the impact of adding a large load at the same location, a base case is simulated. In the base case, a constant power load equivalent to the power drawn by the vehicles is connected in place of the vehicle chargers. All results shown compare the cases of vehicle chargers connected to bus 680 with the base case. [6]

3.2.2 Impacts on the System:

The impact on the system was studied for CCVSC and VCVSC type of the battery charging system with L and LCL type of filters and is described in [6].

3.2.1.1 VCVSC Type of Battery Charger with L Filter:

The VCVSC with L filter shows a negative impact on the system during the period when the fault is cleared from the system and the recloser is still open during a slow cycle. The fault clears from the system at 5.275 s and the recloser remains open until 5.33 s. During this period a high magnitude, high frequency switching voltage is fed back into the system on phase A of bus 680 from the vehicle chargers. The switching voltage on phase A of bus 680 comes from the vehicles connected to phases A and C on the secondary side of the Delta-Wye Grounded transformer. The vehicles on phase B remain largely unaffected due to the connection of the transformer. The peak magnitude of this voltage is over two times the steady state peak voltage. Once the recloser reconnects

phase A of bus 680 to the rest of the distribution system, normal steady state operation resumes. Fig. 3.3 and Fig. 3.4 show the voltage waveforms on phase A of bus 680 during the fault and recovery.

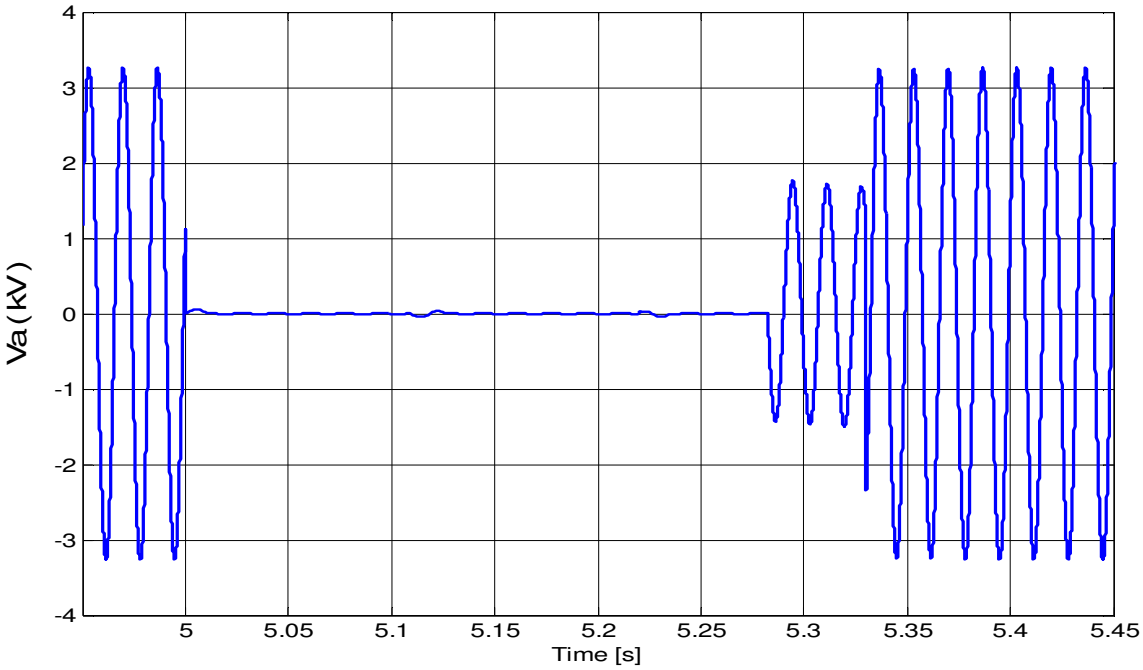

Fig. 3.3- Base Case with Equivalent Load Bus 680 Phase 'A' Voltage

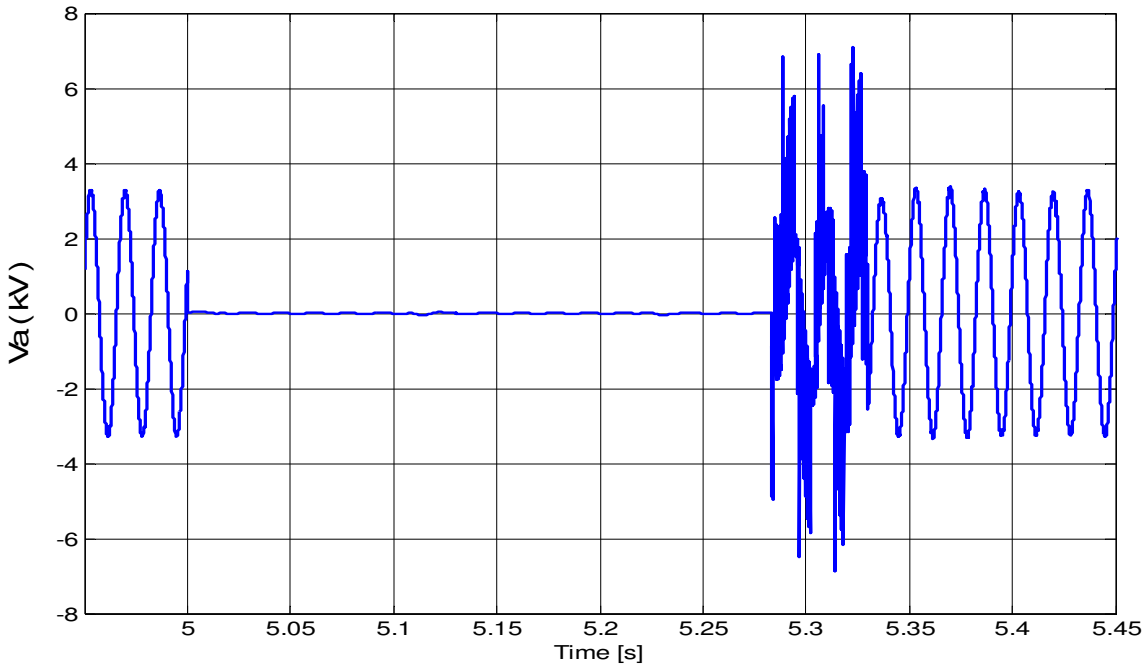

Fig. 3.4- VCVSC Type Battery Charger with L Filter Bus 680 Phase 'A' Voltage

After the recloser reconnects phase A of the distribution system to bus 680, a decaying transient is seen in the current. Fig. 3.5 and Fig. 3.6 show the current waveform of phase B of bus 680 during the fault and recovery. [6]

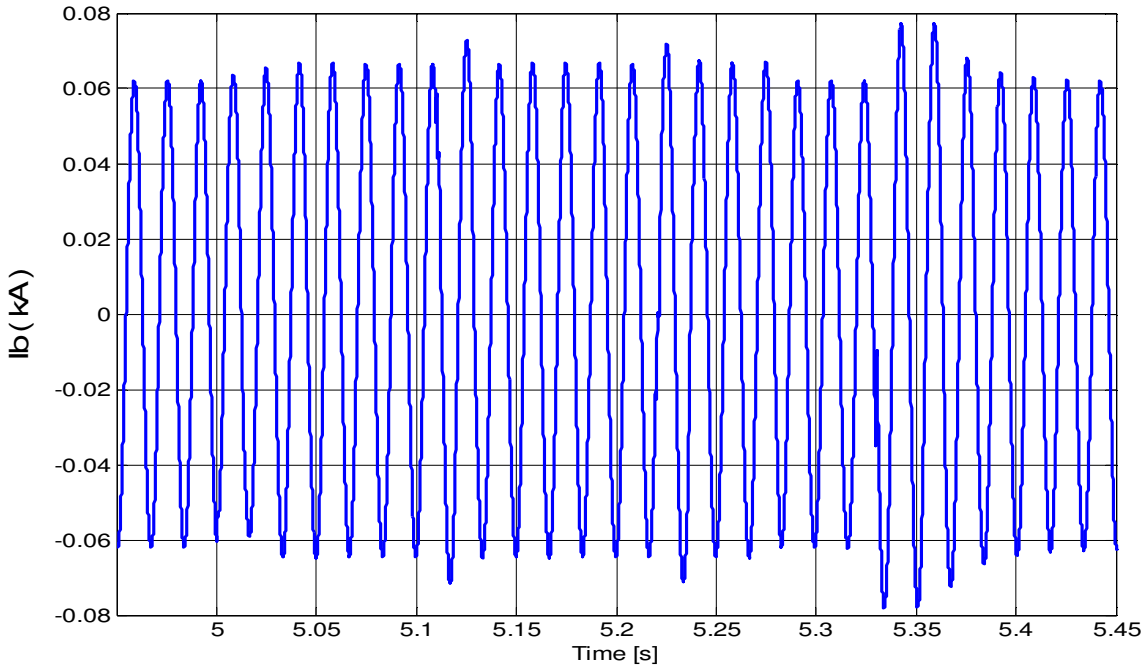

Fig. 3.5- Base Case with Equivalent Load Bus 680 Phase 'B' Current

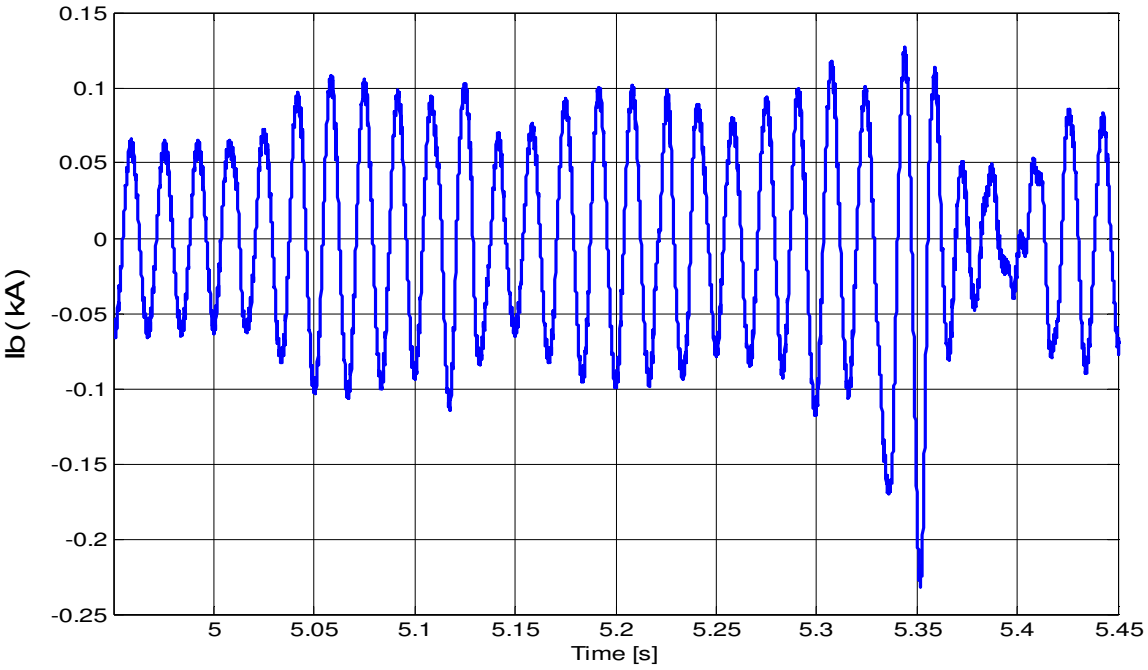

Fig. 3.6- VCVSC Type Battery Charger with L Filter Bus 680 Phase 'B' Current

3.2.1.2 VCVSC Type Battery Charger with L CL Filter:

The VCVSC with LCL filter also shows a negative impact on the system during the same period as the VCVSC with L filter. With this charger model, a similar high magnitude, high frequency switching voltage is fed back into the system on phase A of bus 680. In this case however, the peak magnitude of the switching voltage is comparatively very large as that seen with the L filter and is over nine times the steady state value. Fig. 3.7 and Fig. 3.8 show the voltage waveforms on phase A of bus 680 during the fault and recovery. A similar decaying current transient as observed in case of L filter is also observed with LCL filter. [6]

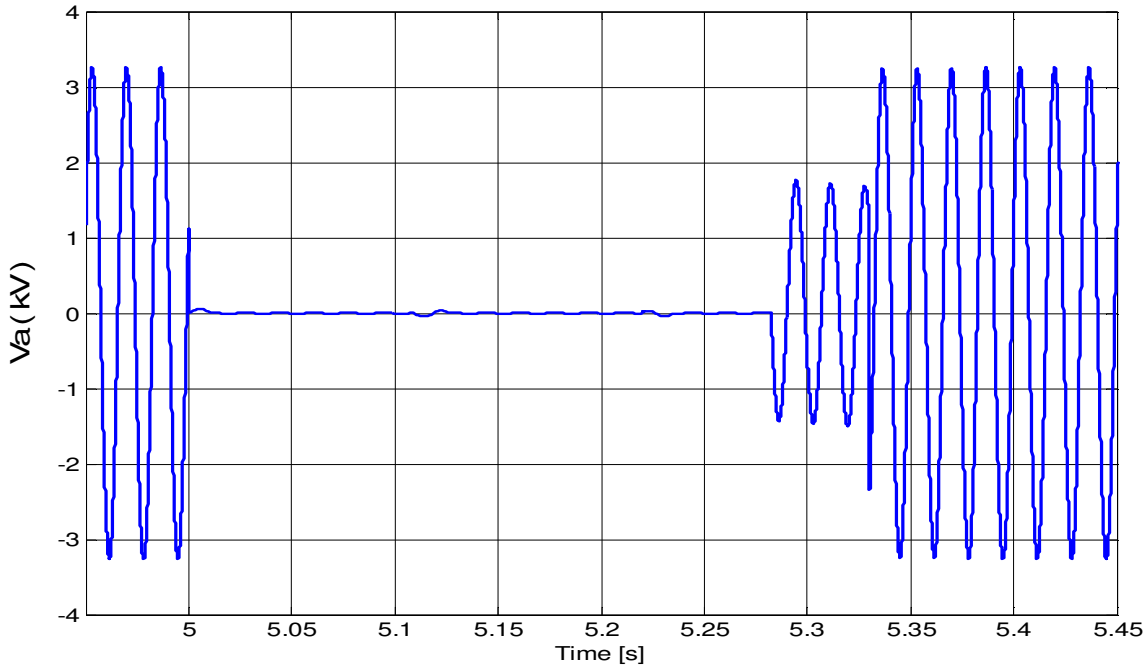

Fig. 3.7- Base Case with Equivalent Load Bus 680 Phase 'A' Voltage

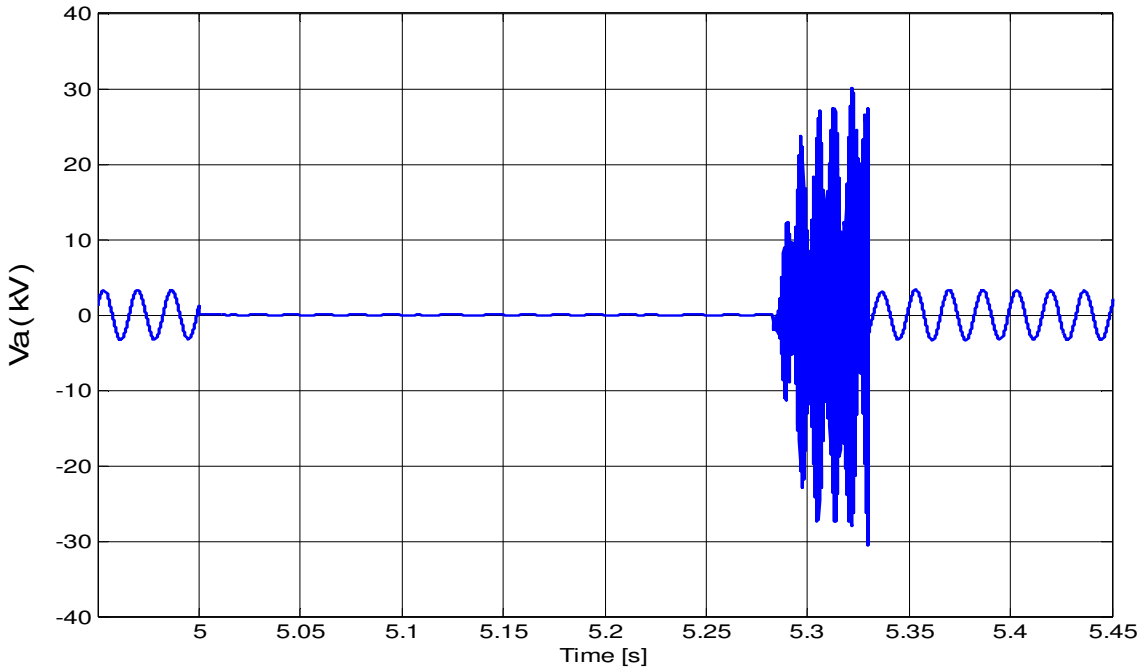

Fig. 3.8- VCVSC Type Battery Charger with LCL Filter Bus 680 Phase 'A' Voltage

3.2.1.3 CCVSC Type Battery Charger with L Filter:

Similar negative impacts as observed for both the types of VCVSC type battery charging system is also shown by CCVSC type battery charger with L filter. Fig. 3.9 and Fig. 3.10 show the voltage waveform of phase A at bus 680 during the fault and recovery. The peak magnitude of the switching voltage is similar to that of the VCVSC with L filter but has a different wave shape. [6]

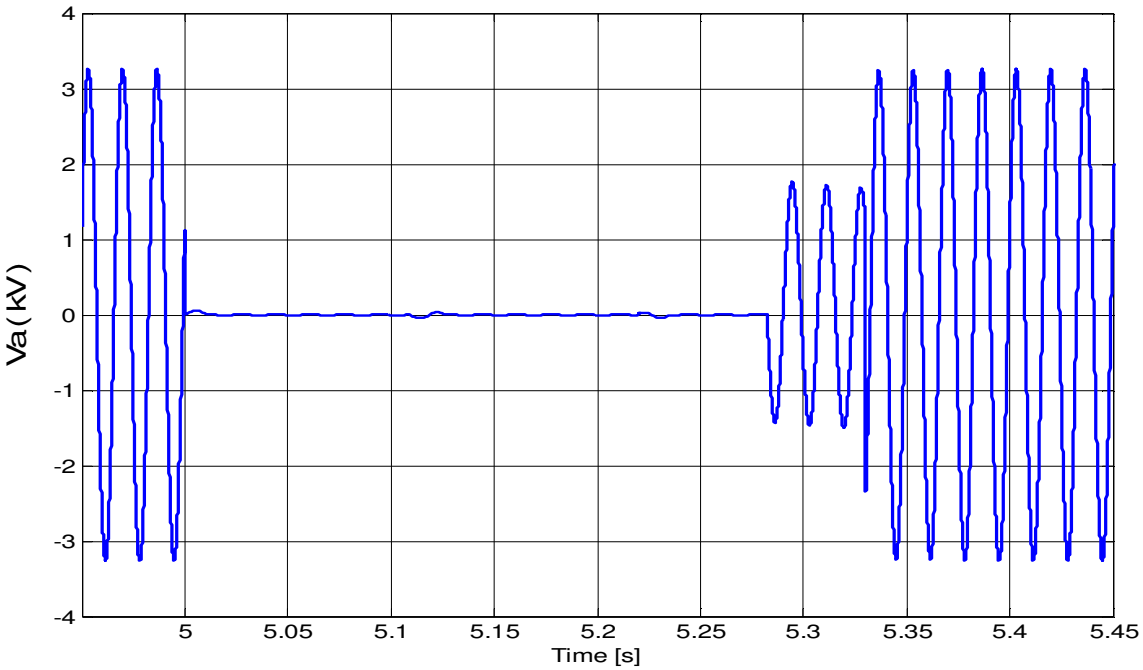

Fig. 3.9- Base Case with Equivalent Load Bus 680 Phase 'A' Voltage

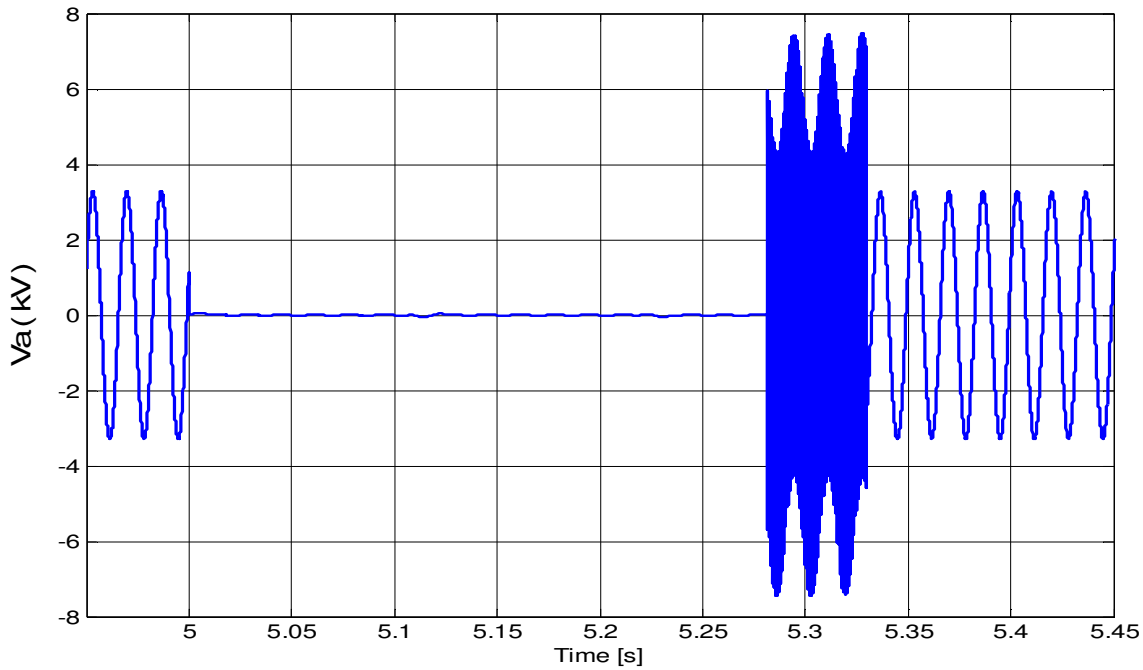

Fig. 3.10- CCVSC Type Battery Charger with L Filter Bus 680 Phase 'A' Voltage

Since CCVSC directly controls the magnitude and waves shape of the current flowing into the charger, the current transient problem observed with VCVSC type of battery chargers is not present with CCVSC. Fig. 3.11 and Fig. 3.12 show the current on phase B of bus 680 during the fault and recovery.

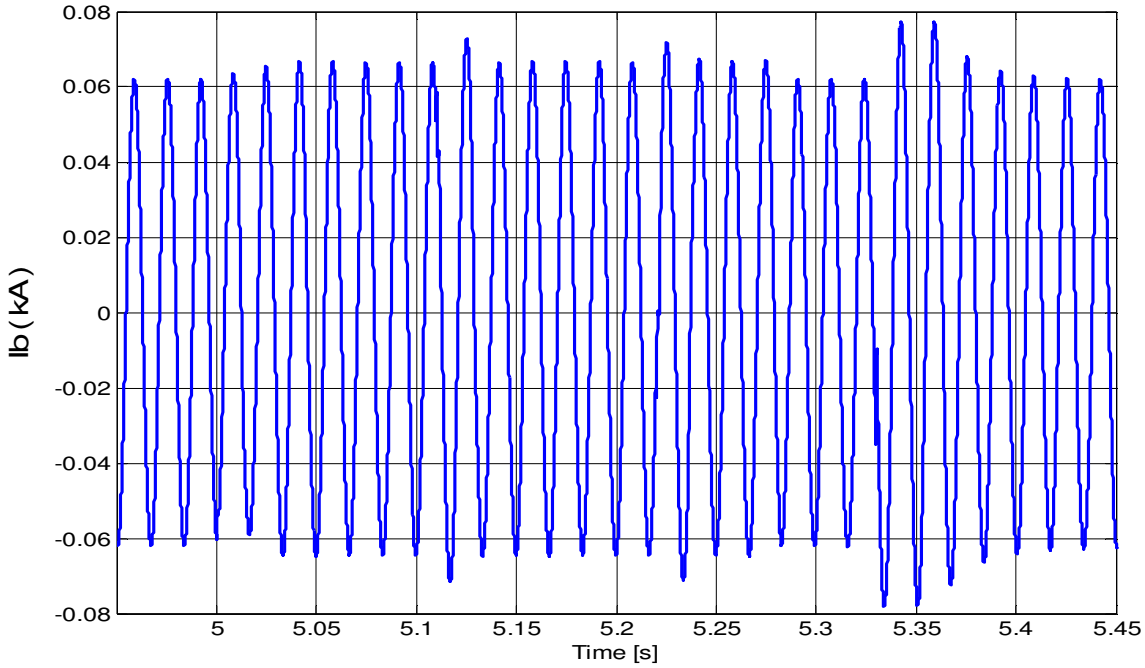

Fig. 3.11- Base Case with Equivalent Load Bus 680 Phase 'B' Current

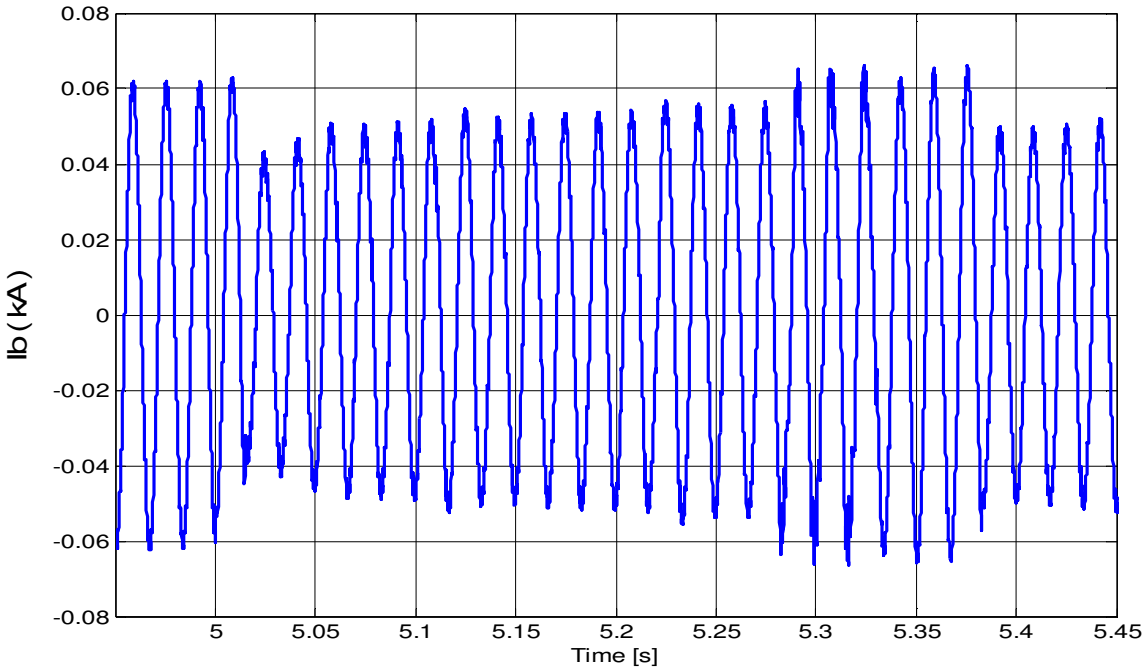

Fig. 3.12- CCVSC Type Battery Charger with L filter Bus 680 Phase 'B' Current

3.2.1.4 CCVSC Type Battery Charger with LCL Filter:

The CCVSC with LCL filter does not show a negative impact on the distribution system during the fault recovery period. Fig. 3.13 and Fig. 3.14 show the voltage waveform on phase A at bus 680 during the fault and recovery. The only difference seen compared to the base case is a small decaying DC offset in the voltage waveform during the period when the fault is cleared from the system and the recloser remains open. As with CCVSC with L filter, no current transients were observed with LCL filter.

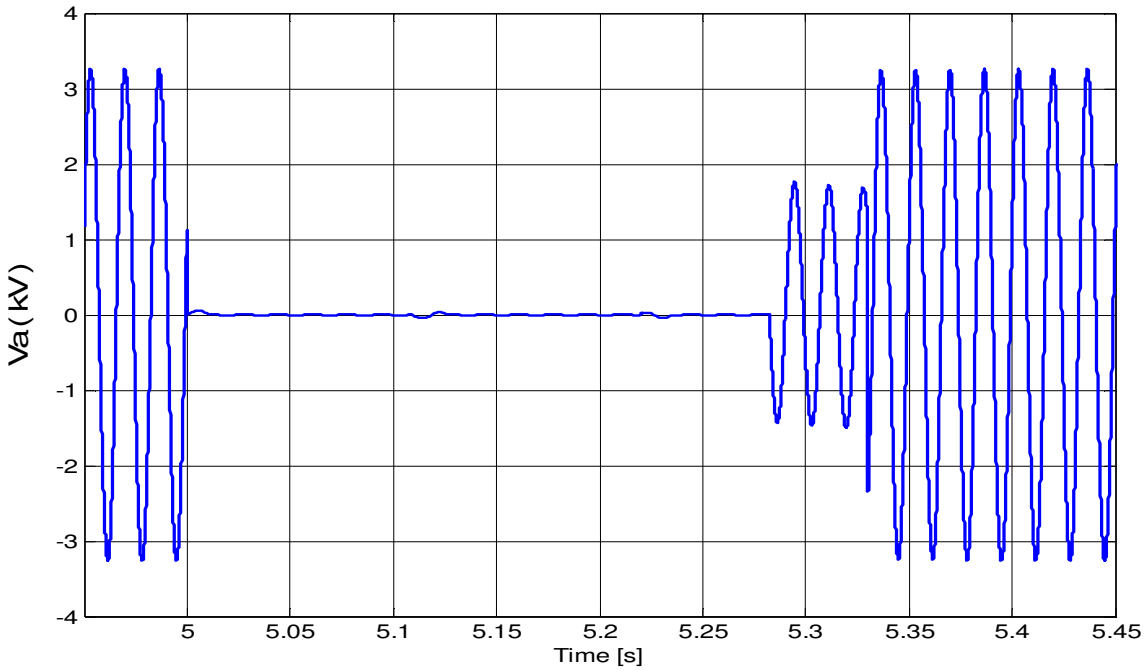

Fig. 3.13- Base Case with Equivalent Load Bus 680 Phase 'A' Voltage

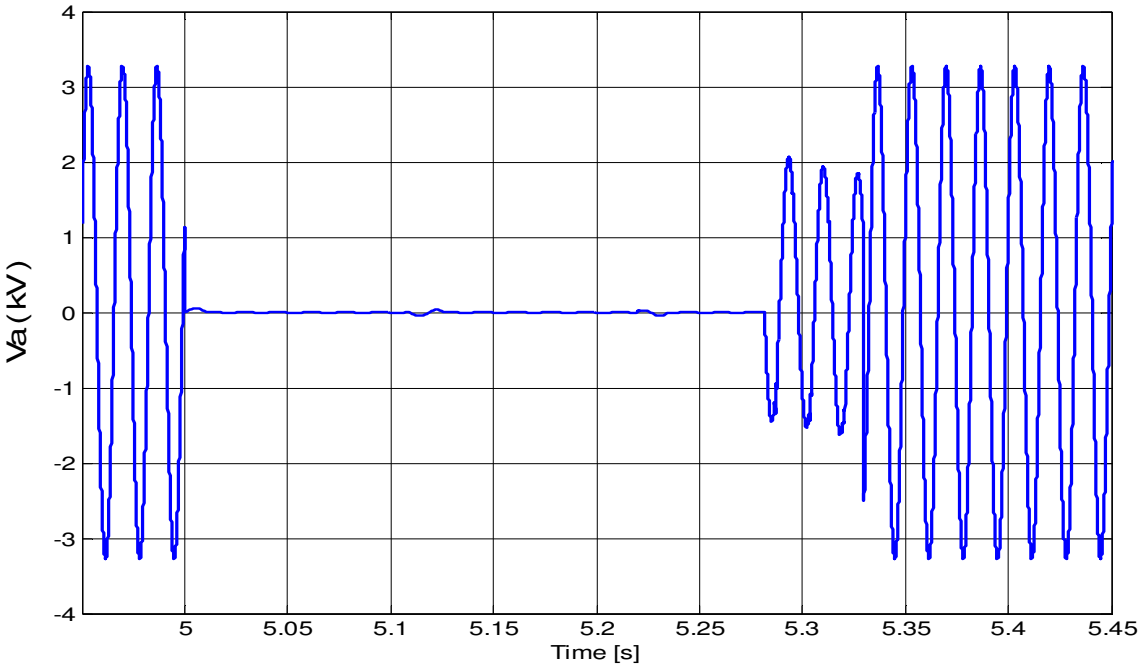

Fig. 3.14- CCVSC Type Battery Charger with LCL Filter Bus 680 Phase 'A' Voltage

3.3 Mitigation of the Impacts with Fault Control Logic:

Based on the negative impacts observed with VCVSC type battery charging system with L and LCL filter and the CCVSC type battery charging system with the L filter, it is desired to implement extra control structures to mitigate the negative impacts. To accomplish this task, control was added to stops all switching in the vehicle charger when the voltage at the terminals of the charger drops below 200V. In per unit, this voltage is well below normal voltage drop limits in a distribution system. During this period where switching is stopped, all switches are left in the open position. After the terminal voltage returns to a normal value, the switching is allowed to resume. This prevents the vehicles from feeding back to the system while the recloser has phase A of bus 680 disconnected from the rest of the distribution system. Fig. 3.15 and Fig. 3.16 show the voltage of phase A at bus 680 of the VCVSC with LCL filter with and without fault control for comparison. With the fault control logic implemented, the vehicle chargers show almost no negative impacts on the distribution system during the fault and recovery. [6]

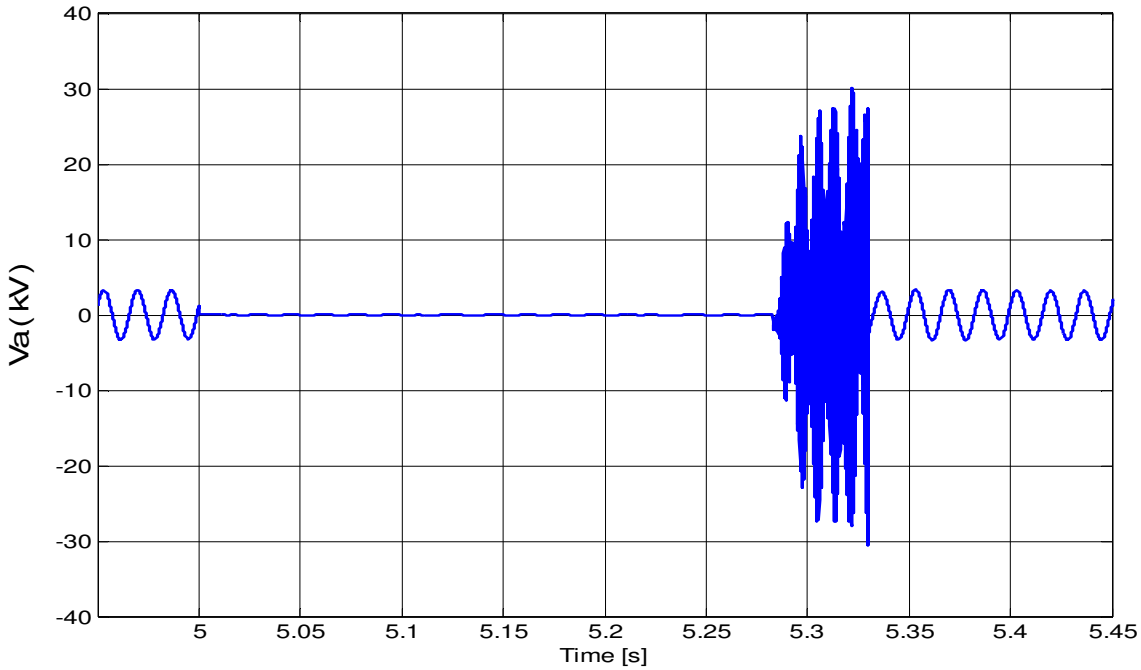

Fig. 3.15- VCVSC Type Battery Charger with LCL Filter Bus 680 Phase 'A' Voltage without Fault Control

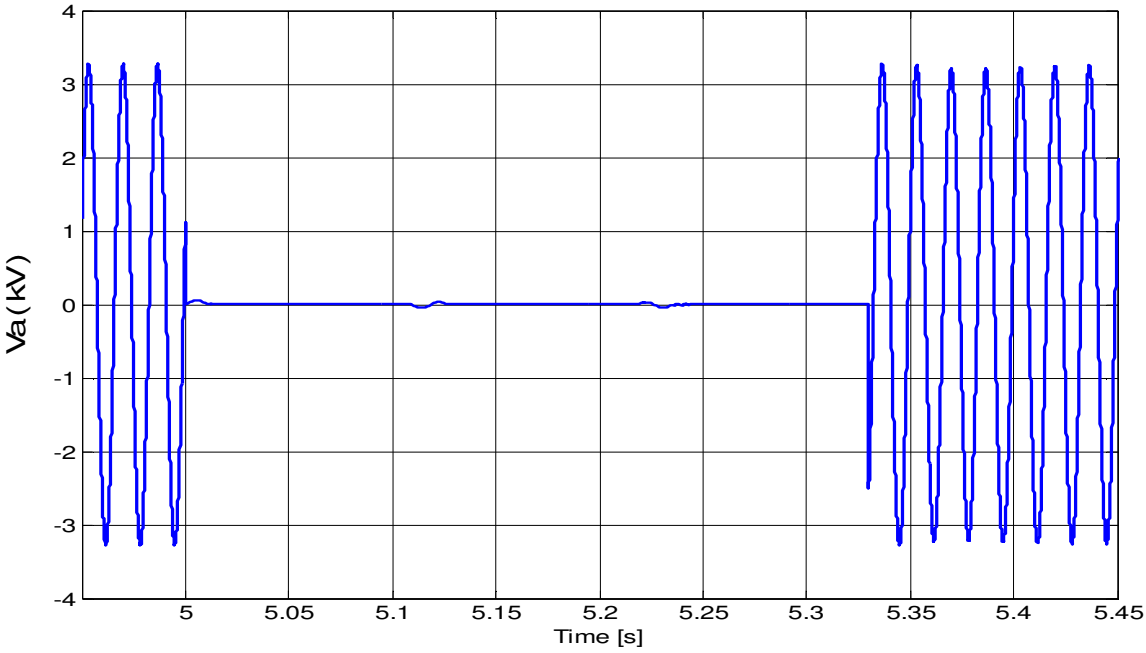

Fig. 3.16- VCVSC Type Battery Charger with LCL Filter Bus 680 Phase 'A' Voltage with Fault Control

3.4 Impacts of PEVs on Distribution System with PV Penetration:

3.4.1 System Description:

The system and the fault analysis performed to determine the impacts of PEVs on the distribution system with PV penetration is the same as that used in section 3.2. Two three phase PVs, each rated for approximately 235 kW were added to the system shown in Fig.3.1 at buses 601,671,633,675 and 680. The total generation by the PVs would satisfy approximately 67% of active power demanded by the loads in the system.

3.4.2 Description of the PV module:

The entire PV module along with its control used for the purpose of the thesis is supplied by PSCAD™/EMTDC™ Customer Support. The details of it can be found in [33] but it has been explained in brief over here for ready reference. The PV module basically consists of a PV array block, a DC/DC converter to implement Maximum Power Point Tracking (MPPT) algorithm and an Inverter to convert DC-Link voltage to an AC voltage with desired magnitude and frequency.

3.4.2.1 PV array block:

The parameters entered in the PV array block are as shown in the Fig. 3.17. There are two variables, Solar Radiation and Cell Temperature, which can be dynamically changed during the simulation. However, considering small simulation time for this study the two variables were fixed at 1200 W/m^2 and 50° C respectively.

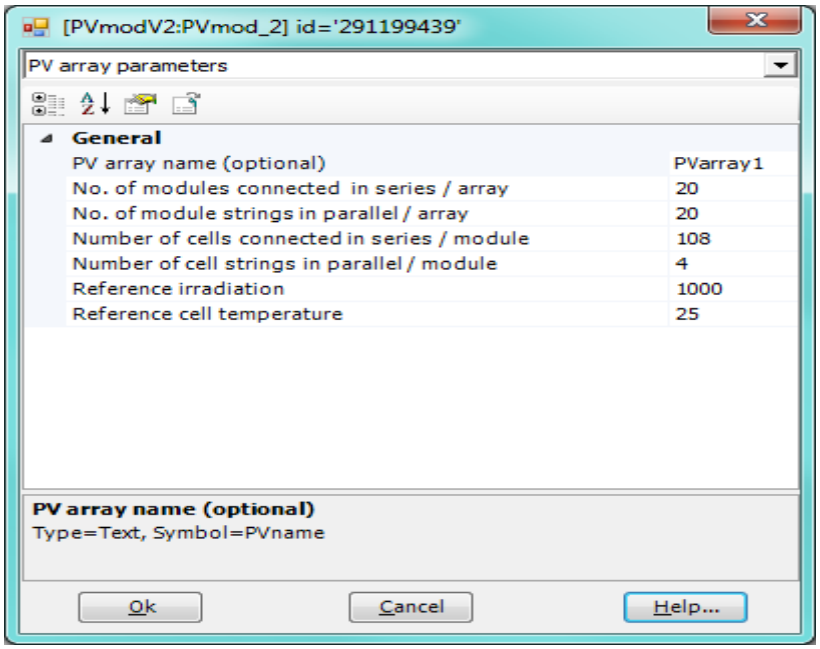

Fig. 3.17- Parameters Entered in PV array Block of PSCAD™/EMTDC™

3.4.2.2 MPPT and DC/DC Converter:

The typical I-V curve for PV cell is as shown in Fig. 3.18. I_{sc} is the short-circuit current, V_{oc} represents the open circuit voltage and Maximum Power Point is denoted by MPP.

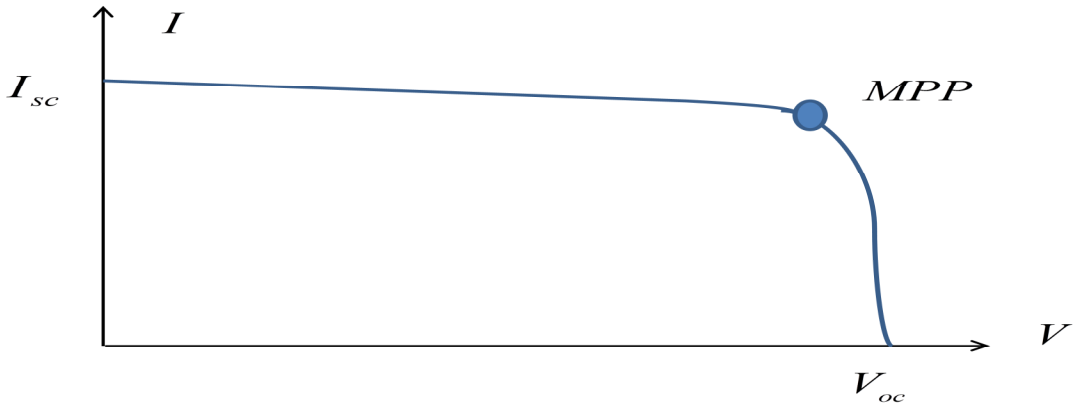

Fig. 3.18- Typical I-V characteristic of PV cell [33]

Based on I-V characteristics, it can be said that, for a given solar radiation and cell temperature there exists a particular voltage at which maximum power can be extracted from the PV module. MPPT algorithm determines the magnitude of voltage at which maximum power would be obtained. The DC-Link voltage is maintained constant by the inverter. The DC/DC converter does the job of converting the DC-Link voltage to the desired voltage at the terminals of the PV module as commanded by the MPPT algorithm.

3.4.2.3 Inverter:

The main job of the inverter is to convert the DC-Link voltage to an AC voltage phasor in a manner that desired power flow to the grid is achieved. The inverter used by PSCAD™/EMTDC™ is a three phase VCVSI. The control of the inverter used by PV module in PSCAD™/EMTDC™ is similar to the direct control methodology described in section 2.1.1

3.4.3 Impacts on the System:

Figures below compares the response of the battery chargers with and without penetration of the PV during the time period when a high magnitude switching voltage was observed on the system as described in section 3.2.1.

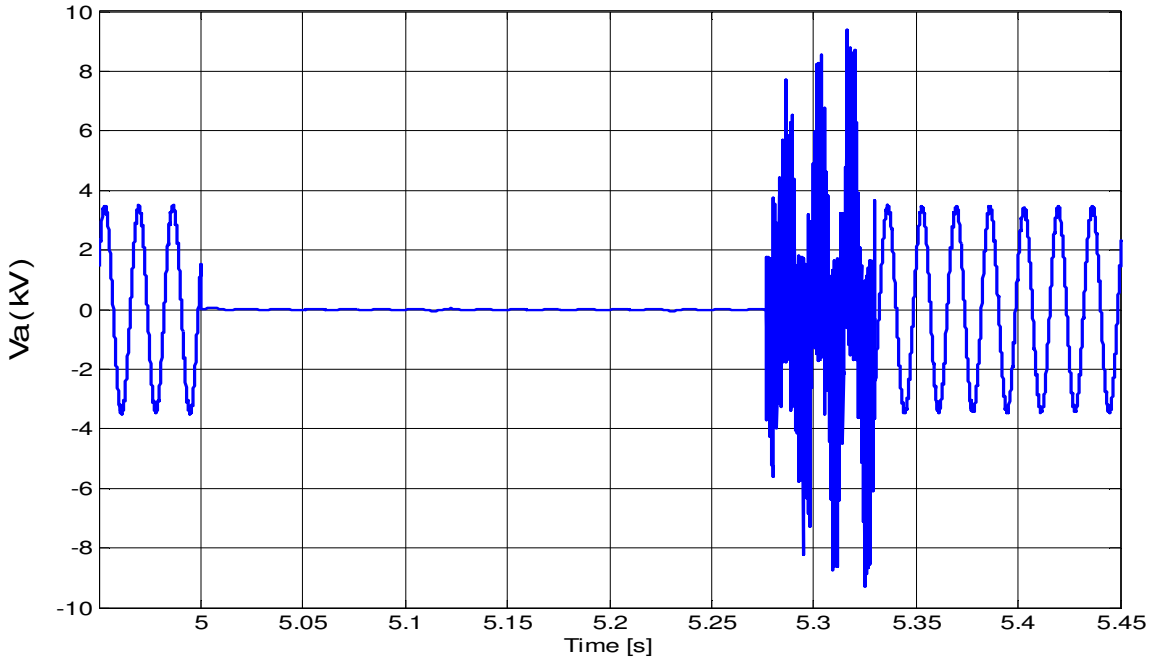

Fig. 3.19- VCVSC Type Battery Charger With L Filter Bus 680 Phase 'A' Voltage With PV penetration

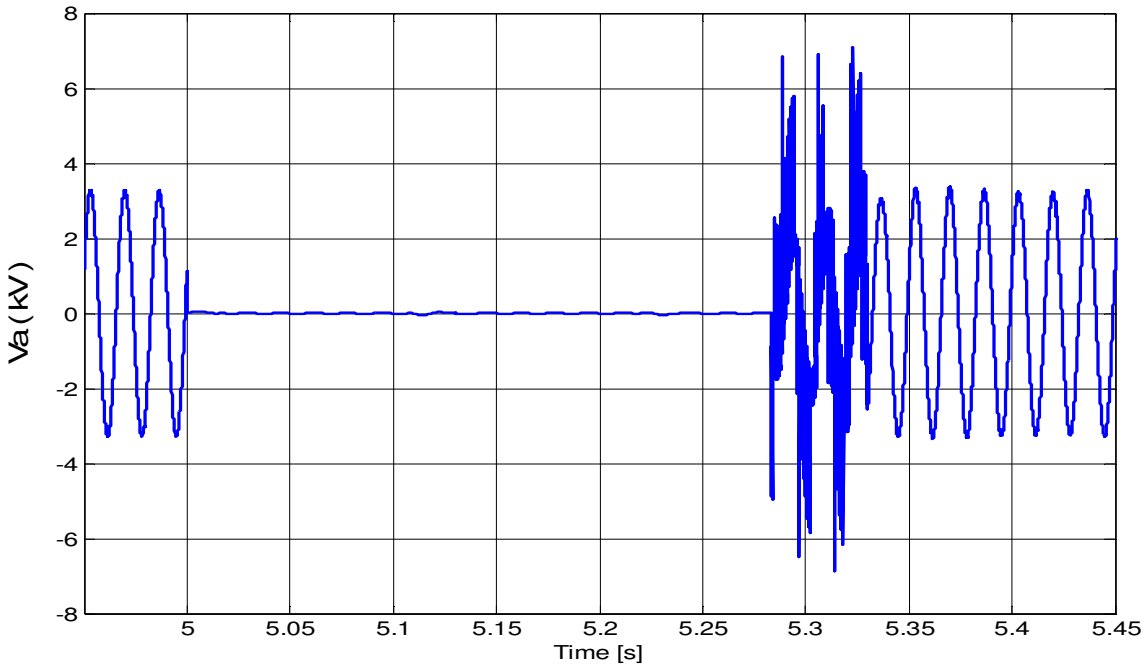

Fig. 3.20- VCVSC Type Battery Charger With L Filter and Bus 680 Phase 'A' Voltage Without PV Penetration

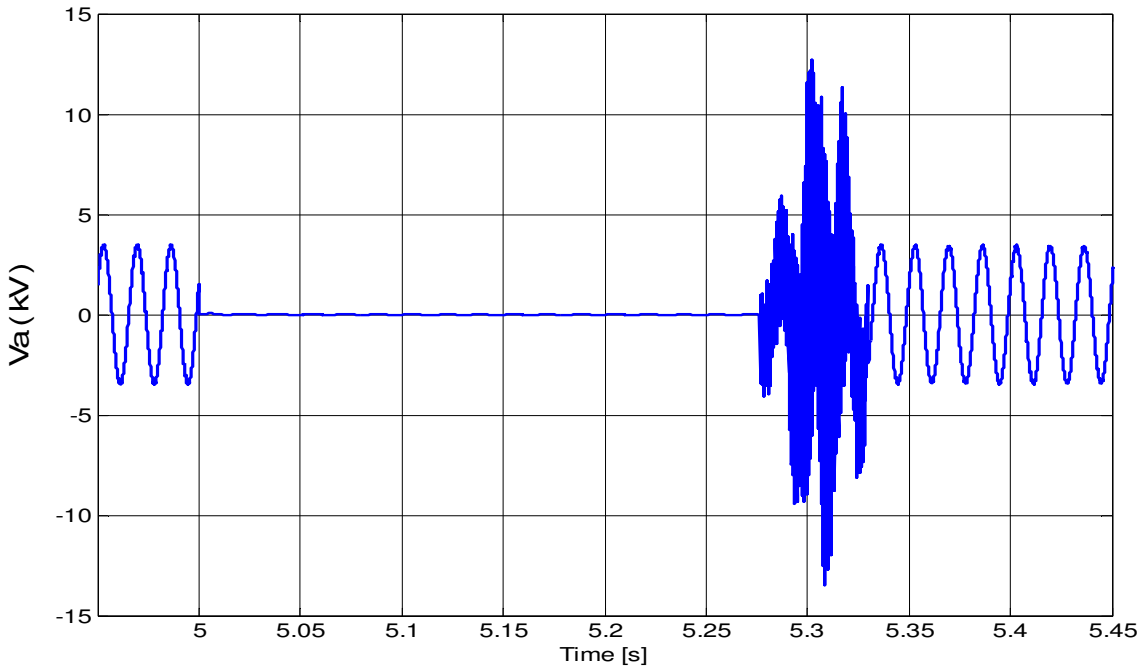

Fig. 3.21- VCVSC Type Battery Charger with LCL Filter Bus 680 Phase 'A' Voltage With PV Penetration

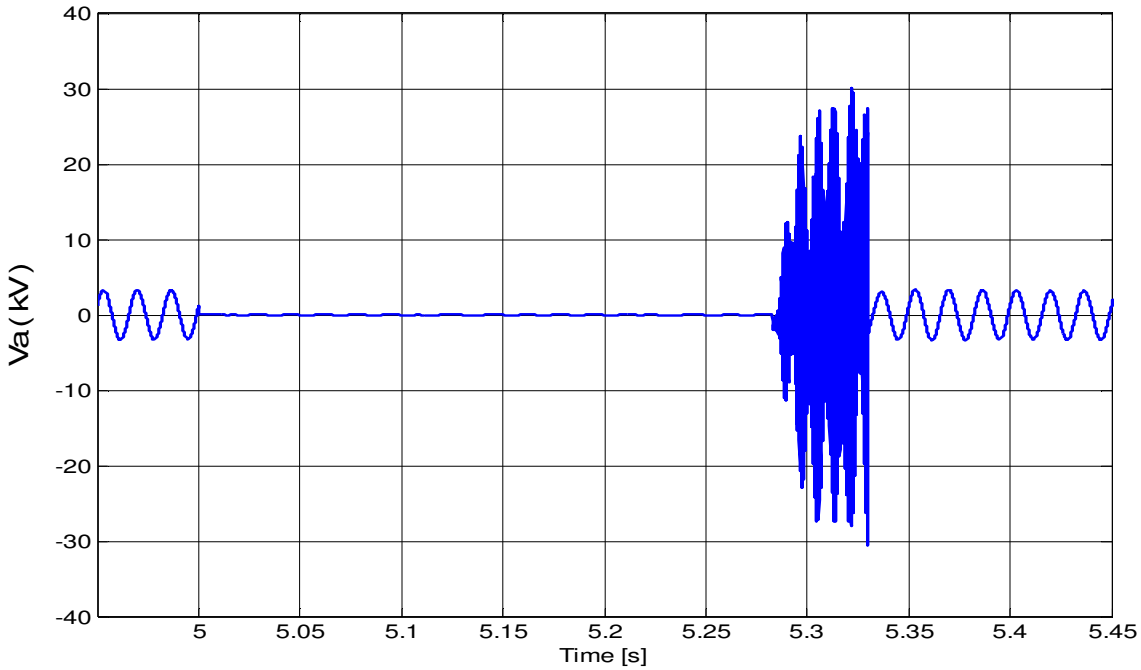

Fig. 3.22- VCVSC Type Battery Charger with LCL Filter Bus 680 Phase 'A' Voltage Without PV Penetration

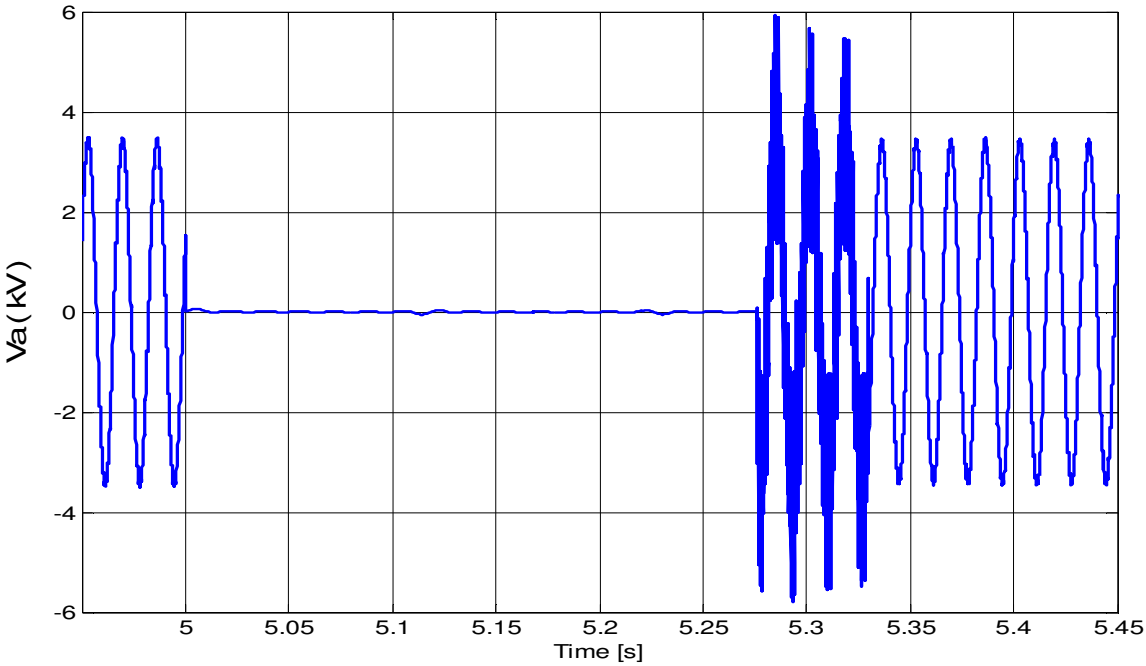

Fig. 3.23- CCVSC Type Battery Charger with L Filter Bus 680 Phase 'A' Voltage With PV Penetration

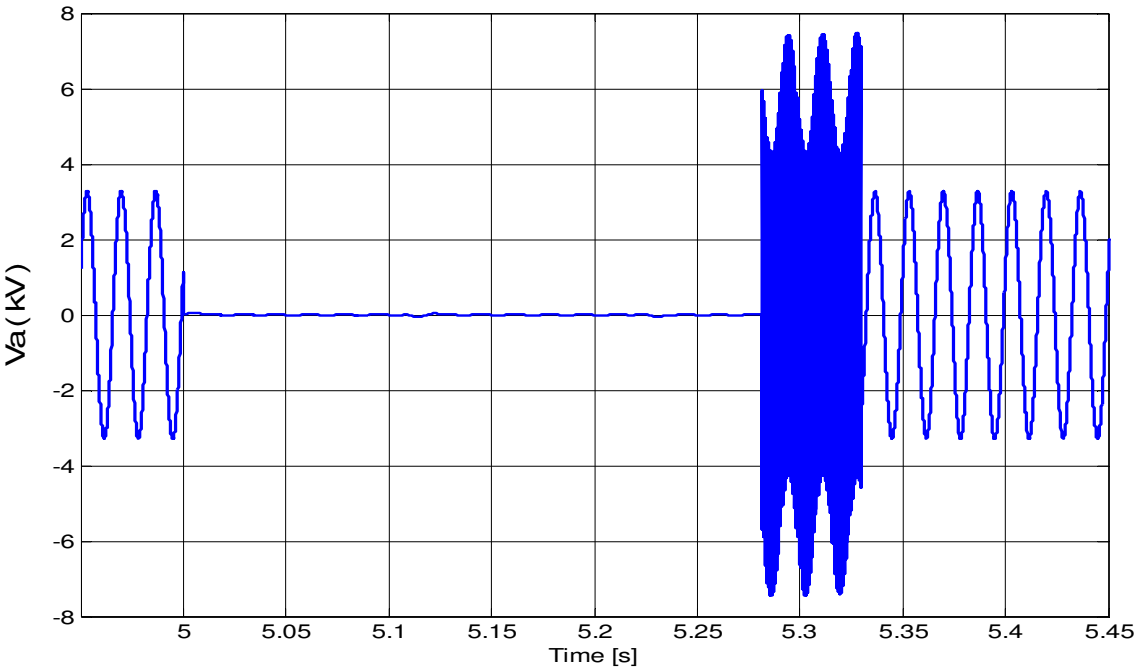

Fig. 3.24- CCVSC Type Battery Charger with L Filter Bus 680 Phase 'A' Voltage Without PV Penetration

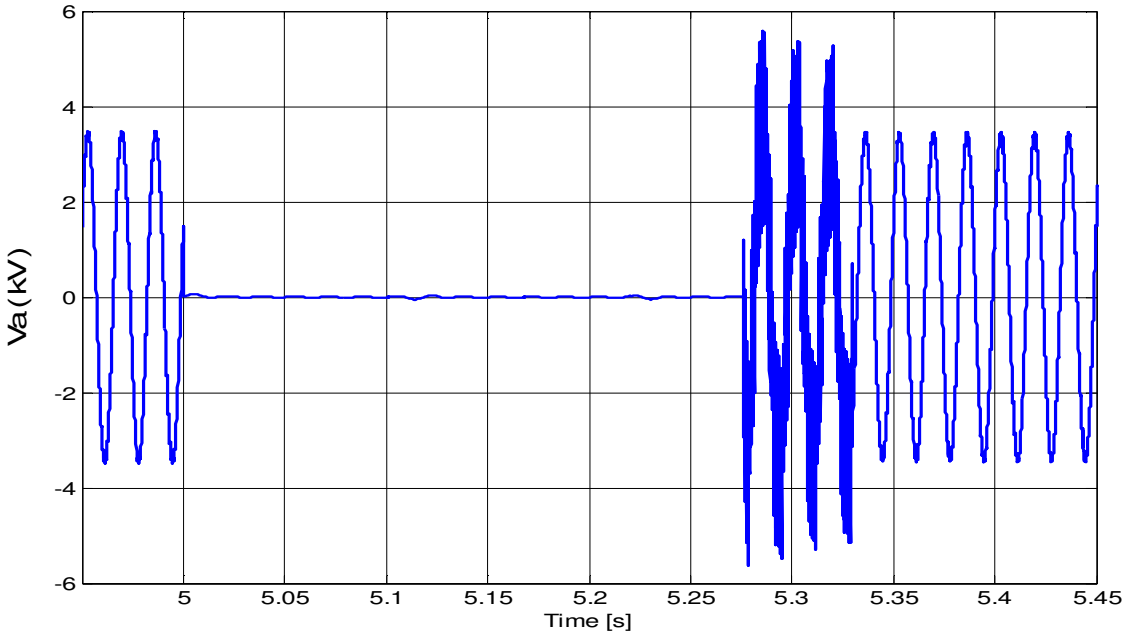

Fig. 3. 25- CCVSC Type Battery Charger with LCL Filter Bus 680 Phase 'A' Voltage With PV Penetration

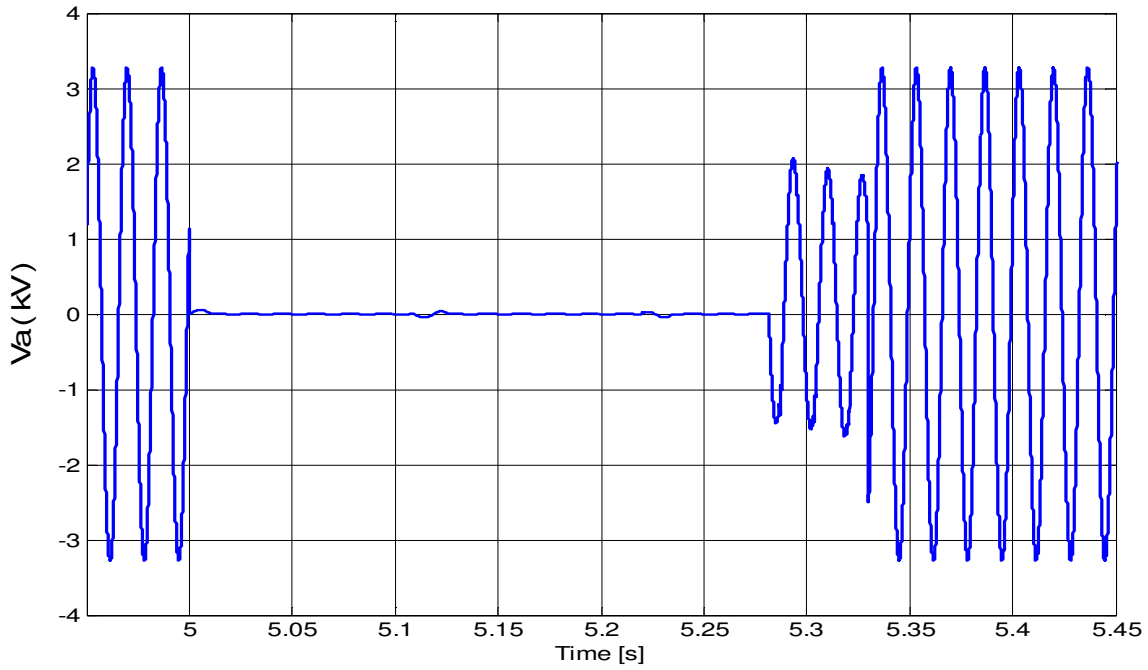

Fig. 3.26- CCVSC Type Battery Charger with LCL Filter Bus 680 Phase 'A' Voltage Without PV Penetration

From the Fig. 3.19 to Fig 3.26, it can be concluded that, in case of system with VCVSC type battery charger with L filter, the high magnitude switching voltage seen on the system during the time when fault has been cleared and reclosure is still open on the phase A of line connecting bus 671 to bus 680, is similar with and without penetration of PV. In case of VCVSC type battery charger with LCL filter, the magnitude of the switching voltage is lower with PV penetration than that seen without PV penetration in the system. The presence of a power source to the vehicles in the form of PV, at bus 680, when the reclosure is open, is the probable reason for reduction in switching voltage magnitude. In case of CCVSC type battery chargers with L and LCL filters, the voltage seen during the period when reclosure is open looks like the one supplied by PV which has a sinusoidal shape but is highly distorted.

3.5 Conclusion:

From the studies conducted on distribution system it can be concluded that without including control in the vehicle chargers to stop switching during a system fault and fault recovery, even a relatively small penetration of PEVs has the potential to significantly impact a distribution system in a negative way. The characteristics of the negative impacts are determined by the control methodology of the PEV charger and the type of input filter implemented. The most dominant among the negative impacts is the high magnitude switching voltage observed during fault recovery. Worst case of this impact occurred with the VCVSC with LCL filter and in contrast, the CCVSC with LCL filter did not produce this impact at all on the distribution system. In order to prevent the potential negative impacts, extra control needs to be added to PEV chargers. In this thesis, a fault control logic which stops switching and keep the switches in open position when the terminal voltage at the charger falls below 200V was implemented. With this extra control, PEVs can be added to a distribution system without presenting a significant risk during faults and fault recovery.

REFERENCES

[1] "Annual Energy Outlook 2012," *U.S. Energy Information Administration*. [Online]. pp. 31-36. Available: http://www.eia.gov/ forecasts/ aeo/pdf/0383(2012).pdf

[2] Clarke, A.; Bihani, H.; Makram, E.; Corzine, K.; "Fault Analysis on an Unbalanced Distribution System in the Presence of Plug-In Hybrid Electric Vehicles," Clemson Power System Conference, 2013

[3] Bunga S.K. (2013). Impact of plug in electric vehicle battery charging on a distribution system. (Order No. 1537069, The University of Tennessee at Chattanooga). ProQuest Dissertations and Theses , 84.Retrieved from http://search.proquest.com

[4] Kisacikoglu M.C., Ozpineci B., and Tolbert L.M., "Examination of a PHEV bidirectional charger system for V2G reactive power compensation," in , 2010 Twenty-Fifth Annual IEEE Applied Power Electronics Conference and Exposition (APEC), vol., no., pp.458-465, 21-25 Feb. 2010

[5] Kisacikoglu, M.C.; Ozpineci, B.; Tolbert, L.M., "Reactive power operation analysis of a single-phase EV/PHEV bidirectional battery charger" Power Electronics and ECCE Asia (ICPE & ECCE), 2011 IEEE 8th International Conference on, vol., no., pp.585, 592, May 30 2011-June 3 2011 doi: 10.1109/ICPE.2011.5944614

[6] Clarke, A.; Bihani, H.; Makram, E.; Corzine, K.; "Analysis and Mitigation of the Impact of Different PEV Battery Chargers during Faults," Submitted to Electric Power Systems Research Journal, Elsevier

[7] Kisacikoglu, M.C.; Ozpineci, B.; Tolbert, L.M.; Wang, F., "Single-phase inverter design for V2G reactive power compensation," Applied Power Electronics Conference and Exposition (APEC), 2011 Twenty-Sixth Annual IEEE , vol., no., pp.808,814, 6-11 March 2011

[8] Gautam, D.; Musavi, F.; Edington, M.; Eberle, W.; Dunford, W.G., "An automotive on-board 3.3 kW battery charger for PHEV application," Vehicle Power and Propulsion Conference (VPPC), 2011 IEEE , vol., no., pp.1,6, 6-9 Sept. 2011

[9] Jaganathan, S.; Wenzhong Gao, "Battery charging power electronics converter and control for plug-in hybrid electric vehicle," Vehicle Power and Propulsion Conference, 2009. VPPC '09. IEEE , vol., no., pp.440,447, 7-10 Sept. 2009

[10] Xiaohu Zhou; Lukic, S.; Bhattacharya, S.; Huang, A., "Design and control of grid-connected converter in bi-directional battery charger for Plug-in hybrid electric vehicle application," Vehicle Power and Propulsion Conference, 2009. VPPC '09. IEEE , vol., no., pp.1716,1721, 7-10 Sept. 2009

[11] Erb, D.C.; Onar, O.C.; Khaligh, A., "An integrated bi-directional power electronic converter with multi-level AC-DC/DC-AC converter and non-inverted buck-boost converter for PHEVs with minimal grid level disruptions," Vehicle Power and Propulsion Conference (VPPC), 2010 IEEE , vol., no., pp.1,6, 1-3 Sept. 2010

[12] Verma, A.K.; Singh, B.; Shahani, D. T., "Grid to vehicle and vehicle to grid energy transfer using single-phase bidirectional AC-DC converter and bidirectional DC-DC converter," Energy, Automation, and Signal (ICEAS), 2011 International Conference on , vol., no., pp.1,5, 28-30 Dec. 2011

[13] Erb, D.C.; Onar, O.C.; Khaligh, A., "Bi-directional charging topologies for plug-in hybrid electric vehicles," Applied Power Electronics Conference and Exposition (APEC), 2010 Twenty-Fifth Annual IEEE , vol., no., pp.2066,2072, 21-25 Feb. 2010

[14] Automotive Energy Supply Corporation [Online]. Available: http://www.eco-aesc-lb.com/en/product/liion_ev/

[15] Sung-Hun Ko; Lee, S.R.; Dehbonei, H.; Nayar, C.V., "Application of voltage- and current-controlled voltage source inverters for distributed generation systems,", IEEE Transactions on Energy Conversion, vol.21, no.3, pp.782,792, Sept. 2006

[16] Lettl, J.; Bauer, J., Linhart, L., “Comparison of Different Filter Types for Grid Connected Inverter,” Progress In Electromagnetics Research Symposium., pp. 1426-1429, 20-23, Mar. 2011

[17] Fain D., “A Dual Input Bidirectional Power Converter for Charging and Discharging a PHEV Battery,” Master’s thesis, Dept. of Elec. and Comp. Eng., Clemson Univ., Clemson, 2009

[18] Sood, V.; Patel, H., "Comparison between direct and vector control strategy for VSC-HVDC system in EMTP-RV," Power Electronics, Drives and Energy Systems (PEDES) & 2010 Power India, 2010 Joint International Conference on , vol., no., pp.1,6, 20-23 Dec. 2010

[19] Tran Cong Binh, Mai Tuan Dat, Ngo Manh Dung, Phan Quan An, Pham, Dinh Truc, Nguyen Huu Phuc, “Active and Reactive Power Controller for Single-Phase Grid- Connected Photovoltaic Systems” , Proceedings of AUN-SEEDNet Conference of Renewable Energy-Bandung-Indonesia, March 2009

[20] Monfared, M.; Sanatkar, M.; Golestan, S., "Direct active and reactive power control of single- phase grid-tie converters," Power Electronics, IET, vol.5, no.8, pp.1544, 1550, September, 2012, doi: 10.1049/iet-pel.2012.0131

[21] Samerchur, S.; Premrudeepreechacharn, S.; Kumsuwun, Y.; Higuchi, K., "Power control of single-phase voltage source inverter for grid-connected photovoltaic systems," Power Systems Conference and Exposition (PSCE), 2011 IEEE/PES , vol., no., pp.1,6, 20-23 March 2011

[22] Ciobotaru, M.; Teodorescu, R.; Blaabjerg, F., "A New Single-Phase PLL Structure Based on Second Order Generalized Integrator," Power Electronics Specialists Conference, 2006. PESC '06. 37th IEEE , vol., no., pp.1,6, 18-22 June 2006

[23] Chiniforoosh, S. (2007). "Generalized Dynamic Average Value Modeling of Line-Commutated Converter Systems In Transient Simulation Programs", The University of British Columbia, Vancouver, Retrieved from https://circle.ubc.ca/

[24] Darabi, Z.; Ferdowsi, M., "Aggregated Impact of Plug-in Hybrid Electric Vehicles on Electricity Demand Profile,", IEEE Transactions on Sustainable Energy , vol.2, no.4, pp.501, 508, Oct.2011 doi: 10.1109/TSTE.2011.2158123

[25] Hilshey, A.D.; Hines, P.D.H.; Rezaei, P.; Dowds, J.R., "Estimating the Impact of Electric Vehicle Smart Charging on Distribution Transformer Aging,", IEEE Transactions on Smart Grid, vol.4, no.2, pp.905,913, June 2013

[26] Sortomme, E.; Hindi, M.M.; MacPherson, S.D.J.; Venkata, S.S., "Coordinated Charging of Plug-In Hybrid Electric Vehicles to Minimize Distribution System Losses,", IEEE Transactions on Smart Grid , vol.2, no.1, pp.198,205, March 2011

[27] Pieltain Fernández, L.; Román, T.G.S.; Cossent, R.; Domingo, C.M.; Frías, P., "Assessment of the Impact of Plug-in Electric Vehicles on Distribution Networks,", IEEE Transactions on Power Systems , vol.26, no.1, pp.206,213, Feb. 2011 doi: 10.1109/TPWRS.2010.2049133

[28] Sekyung Han; Soohee Han; Sezaki, K., "Development of an Optimal Vehicle-to-Grid Aggregator for Frequency Regulation,", IEEE Transactions on Smart Grid, vol.1, no.1, pp.65,72, June2010 doi: 10.1109/TSG.2010.2045163

[29] Sortomme, E.; El-Sharkawi, M.A., "Optimal Scheduling of Vehicle-to-Grid Energy and Ancillary Services," IEEE Transactions on Smart Grid, , vol.3, no.1, pp.351,359, March 2012 doi: 10.1109/TSG.2011.2164099

[30] Ruifeng Yan; Saha, T.K., "Investigation of Voltage Stability for Residential Customers Due to High Photovoltaic Penetrations,", IEEE Transactions on Power Systems vol.27, no.2, pp.651,662, May2012 doi: 10.1109/TPWRS.2011.2180741

[31] "IEEE 13 Node Test Feeder," IEEE PES Distribution System Analysis Subcommittee. [Online]. Available: http://ewh.ieee.org/soc/pes/dsacom/ testfeeders/feeder13.zip

[32] "Radial Distribution Test Feeders," IEEE PES Distribution System Analysis Subcommittee.
[Online], Available:http://ewh.ieee.org/soc/pes/dsacom/testfeeders/testfeeders.pdf

[33] Rajapakse, A.D.; Muthumuni, D., "Simulation tools for photovoltaic system grid integration studies," Electrical Power & Energy Conference (EPEC), 2009 IEEE, vol., no , pp.1,5,22-23 Oct.2009 doi: 10.1109/EPEC.2009.5420370